Thomas White

Plasma-assisted Ignition and Combustion for I.C. Engines

Metropolia University of Applied Sciences

Bachelor of Engineering

Automotive Engineering

Bachelor's Thesis

5 May 2023

Abstract

Author:	Thomas White
Title:	Plasma-assisted Ignition and Combustion for IC Engines
Number of Pages:	70 pages + 1 appendices
Date:	5 May 2023
Degree:	Bachelor of Engineering
Degree Programme:	Degree Programme in Automotive Engineering
Professional Major:	Vehicle electronics
Supervisors:	Pasi Kovanen, Senior Lecturer

For gasoline internal combustion engines, the use of plasma-assisted ignition and combustion systems offer many advantages when compared to conventional inductive-discharge or capacitive-discharge ignition systems. In this thesis, the theoretical background pertaining to conventional inductive-discharge and capacitive-discharge ignition systems, the principles of ignition spark formation, the properties of plasma, the development of plasma ignition systems and their properties have been reviewed extensively by consulting the relevant published literature.

Additionally, a patented circuit designed to produce an enhanced discharge, where a spark discharge typical of capacitive discharge ignition systems is augmented with a high-current, low-voltage discharge component, was replicated, tested, and analysed based on identifiable characteristics found in the literature. Based on the results of the tests and analysis conducted, the discharge produced by the replicated circuit was found to strongly resemble that produced by a plasma jet ignition system.

Keywords: plasma-assisted ignition and combustion, plasma jet ignition

Tiivistelmä

Tekijä:	Thomas White
Otsikko:	Plasma-Assisted Ignition and Combustion for IC Engines
Sivumäärä:	70 sivua + 1 liitettä
Aika:	5.5.2023
Tutkinto:	Insinööri (AMK)
Tutkinto-ohjelma:	Ajoneuvotekniikan tutkinto-ohjelma
Ammatillinen pääaine:	Autosähkötekniikka
Ohjaajat:	Lehtori Pasi Kovanen

Bensiinipolttomoottoreissa plasma-avusteisten sytytysjärjestelmien käyttö tarjoaa monia etuja verrattuna perinteisiin induktiivisiin tai kapasitiivisiin akkusytytysjärjestelmiin. Tässä opinnäytetyössä tarkastellaan perinteisten induktiivisten ja kapasitiivisten akkusytytysjärjestelmien teoreettista taustaa, sytytyskipinän muodostumisen periaatteita, plasman ominaisuuksia, plasmasytytysjärjestelmien kehitystä ja niiden ominaisuuksia. Työ perustuu laajaan kirjallisuusaineistoon.

Lisäksi yhtä patentoitua plasmasytytysvirtapiiriä jäljiteltiin, testattiin ja analysoitiin kirjallisuudesta löydettyjen tunnistettavien ominaisuuksien perusteella. Virtapiiri suunniteltiin tuottamaan tehostettua purkausta, jossa kapasitiivisille purkaussytytysjärjestelmille tyypillistä kipinäpurkausta täydennetään suurvirta-pienjännitteisellä purkauskomponentilla.

Tarkastellun virtapiirin tuottaman sytytyskipinän havaittiin tämän opinnäytetyön yhteydessä tehtyjen kokeiden perusteella muistuttavan voimakkaasti plasmasuihkusytytysjärjestelmän tuottamaa purkausta.

Avainsanat: plasma-avusteisten sytytys ja poltto, plasmasuihkusytytys

Contents

1 Introduction

The purpose of this thesis is to investigate the possible advantages and disadvantages a plasma assisted ignition (PAI) or plasma assisted combustion (PAC) system has over more conventional inductive- or capacitive-discharge ignition systems for gasoline internal combustion engines (ICEs). An understanding of the physics of spark ignition and the discharge modes that it is composed of, along with the physics of plasma and its influence on ignition and combustion in the context of electrical discharges produced by ignition systems designed for internal combustion engines is sought out. To achieve this, the theoretical background of the aforementioned topics, in addition to conventional inductive discharge and capacitive discharge ignition systems, will be investigated, and published literature pertaining to these will be reviewed. A patented circuit designed to produce a better ignition spark by adding an energy efficient high current, low voltage component to the spark's discharge plasma is replicated, and based on the reviewed literature, an analysis of results obtained from tests performed to investigate and characterise the circuit's behaviour is performed.

2 Theoretical Background

2.1 Battery Powered Ignition: an Overview

Battery powered ignition has been a mainstay of the gasoline internal combustion engine equipped automobile for more than 110 years and is still standard equipment in todays highly advanced engines (1, p. 143). Although the sophistication of this type of ignition system's componentry has evolved over time, the fundamental elements required for successful operation have not changed and remain true to the earliest designs: the electrical circuit consists of a 12 V battery, an ignition coil (also known as an induction coil) or coils, ignition leads, spark plugs and a means for distributing the ignition coil's output energy to the correct spark plug at a specific moment in time corresponding to desired engine performance.

To establish a point of reference in this study and for the purpose of later comparisons and more detailed analyses of arc discharge phenomena pertaining to spark ignition (SI), attention will be firstly given to the operating principles of the most common battery ignition systems: inductive discharge ignition and capacitive discharge ignition. Both systems rely on the ignition coil to produce the voltage required for arc discharge formation between the electrodes of the spark plug. The operating principle of both systems, with respect to the utilisation of the ignition coil will be described in more detail as follows.

2.1.1 Operating Principles of Inductive-Discharge Ignition

In the inductive-discharge ignition system (IDI), current flow from the battery to the primary windings of the ignition coil is initiated by closing the ignition/starter switch. Battery voltage is typically in the range of 13.4 – 14.2 V, depending on the voltage regulation of the alternator. A magnetic field is thus built up in the primary windings, until, by the action of a triggering mechanism (be it mechanical or electronic) calibrated to switch at a specific moment according to the firing order of the engine, current flow to the coil's primary windings is interrupted, causing the magnetic field to collapse. This change in current and thereby change in magnetic field induces a voltage in the secondary windings of the coil, whose magnitude is determined by the input current, ratio of ignition coil's primary windings to its secondary windings and dwell time (time available for charging) (1, p. 153). Depicted in Figure 1 is a basic schematic of a conventional IDI system.

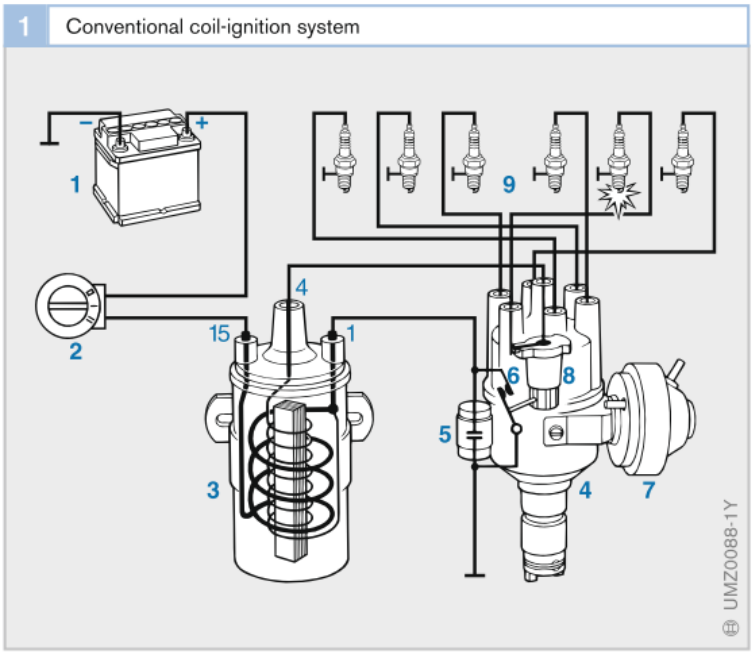

Fig. 1
1 Battery
2 Ignition/starter switch
3 Ignition coil
4 Distributor
5 Capacitor
6 Contact-breaker points
7 Vacuum advance mechanism
8 Rotor
9 Spark plug
1, 4, 15 Terminals

Figure 1. Basic schematic of conventional IDI system (3).

To guarantee electric arc formation in all conditions, the modern IDI system must be able to produce more than 20 kV output voltage (2, p. 349). The induced high voltage is conducted to the appropriate spark plug either directly (in the case of modern coil-on-plug systems) or indirectly (in the case of traditional distributor-based systems). Because of the voltage's magnitude, the dielectric strength of the insulating material between the spark plug's two electrodes is overcome (dielectric strength of air is approximately 3 x 10^6 V/m) and a path for current to flow forms, ultimately manifesting itself as a spark. (1, p. 153; 2, p. 349; 3, 4, p. 630).

2.1.2 Operating Principles of Capacitive-Discharge Ignition

Principally, the capacitive-discharge ignition (CDI) system stores ignition spark energy in the electric field of a capacitor as opposed to the magnetic field of the inductor (ignition coil) in the IDI system. It otherwise shares many features with the IDI system; however, it differs specifically in the mechanism employed to induce output voltage. Current does not flow directly from the battery to the primary windings of the ignition coil, rather a capacitor is first charged to 300 -

500 V and then discharged into the primary windings. Because of the sudden high voltage discharge, magnetic flux rapidly builds up in the coil's primary windings, and as a result the induced voltage in the secondary windings can exceed 40 kV in magnitude (5, p. 1926; 6, p. 4).

In general, the most basic iterations of CDI systems can be said to be comprised of three distinct circuits: a charging circuit, a discharging circuit, and a distribution circuit which is essentially shared with the IDI system (2, p. 402). Battery current is first delivered to a bipolar transistor- or MOSFET-based inverter, after which it is passed to a transformer to raise the voltage. A capacitor is then charged via a full-wave bridge rectifier. When ignition is required, a thyristor is triggered to create a path for the capacitor to discharge into the primary windings of the ignition coil. Under the circumstances the ignition coil behaves more like a pulse transformer than an energy storage device (5, p. 1926). The spark produced by a CDI system is very short in duration; 0,1 – 0.3 ms, owing to the rapid rate with which the system's capacitor discharges (2, p. 401; 5, p. 1926).

2.1.3 Advantages and Disadvantages of IDI, CDI

IDI and CDI systems produce inherently different sparks. As has been previously mentioned, the CDI system produces a spark whose duration is extremely short. The detrimental effects of this can, however, be somewhat compensated for by increasing the size of the gap between the spark plug's electrodes, which is possible due to the significantly higher output voltage produced by CDI (1, p 153; 2, p. 401).

CDI also has an advantage over IDI in terms of 'dwell time' or time required to charge the primary windings of the ignition coil. A CDI system's ignition energy does not depend on the inductance of the ignition coils primary windings, rather it is dependant on the properties of the system's discharge capacitor. Available ignition energy can be defined as:

$$E = \frac{C \cdot U^2}{2} \tag{1}$$

C is the capacitors capacitance in farads.
U is the capacitors voltage in volts.

The capacitor's charge time is independent of engine speed. A charge time of 0.3 ms is a little less than one tenth of the time required for the current in the primary winding of an IDI system's ignition coil to reach its set-point value (1, p. 153; 2, p. 401; 5, p. 1926). Furthermore, by dint of the exceptionally rapid rise time of the CDI system's output voltage over the spark plug's electrodes, contaminated or fouled spark plugs do not significantly hinder the performance of a CDI system (2, p. 401).

Despite these advantages, CDI has not been broadly adopted by the automotive industry. Compared to IDI, CDI is more expensive and relatively complex (2, p. 402). Conversely, transistor assisted IDI systems with longer spark durations were introduced to ensure that lean mixtures did burn properly. Modern electronic IDI systems also allow the regulation of spark duration depending on engine operating conditions. (7, p. 104).

2.2 Principles of Ignition Spark Formation

In an internal combustion engine, if the engine's ignition system is unable to meet the demands of its operating environment and certain performance criteria, the ignition spark will not have the proper characteristics or not form at all. Consequently, ignition will not take place and misfiring will result (8, p. 9). The spark must be of sufficient energy and duration to ensure that a self-sustaining combustion reaction is initiated in the combustible mixture within the combustion chamber (9, p. 1). According to Maly, the spark consists of three distinct phases: breakdown, arc discharge and glow discharge. Each phase uniquely influences the process of self-sustaining combustion reaction formation (10, p. 95).

2.2.1 Breakdown

During the breakdown phase, electron multiplication enables the release of a large amount of electrical energy in a few nanoseconds. This is due to the

formation of conductive plasma in an otherwise insulating medium, the mixture of air and fuel vapour, occupying the gap between the electrodes of the spark plug (11, p. 2). The first stage of breakdown is characterised initially by a very high spark current and high voltage (several hundreds or even thousands of amperes). The breakdown voltage is usually on the order of 20 – 40 kV but can be greater (11, p. 2; 12, p. 1). The value of the spark current is limited by the ignition voltage and the specific impedances of the near gap circuit (comprised of the spark plug and spark plug leads) (10, p. 94).

Simultaneously, the electrical field strength and voltage across the gap decrease sharply to values in the range of 1 kV/cm and $\leq$ 100 V respectively, and, hence, the process garners its name 'breakdown'. The outcome of this phase is specifically determined by the capacitive (5-15 pF) and inductive ($\cong$ 5 nH) properties of the spark plug and spark. For the initiation of a complete breakdown, the minimum energy required at 1 bar and with a 1 mm electrode gap is 0.3 mJ (10, p. 97). Three models can describe breakdown formation processes comprehensively: the Townsend mechanism (over-exponential avalanche multiplication mechanism), Paschen's law and the streamer mechanism (11, p. 2).

2.2.2 Breakdown Models: Townsend Mechanism

The Townsend mechanism was named after John Sealy Townsend, who discovered the fundamental ionisation mechanism by his work between 1897 and 1901 (13). The air-fuel mixture occupying the gap between the two electrodes of the spark plug already contains a number of free electrons as a result of naturally occurring ionising radiations (UV-light, cosmic rays for example) (10, p. 96). When a sufficiently strong electric field is applied across the gap, free electrons are forced to move from the cathode towards the anode (9, p. 6; 10, p. 96). If the electric field is strong enough the accelerated electrons can ionise air molecules by collisions, generating two more free electrons (14, p. 4). The newly generated free electrons' initial velocity is low; however, they too are sufficiently accelerated by the electric field to ionise two more gas molecules, thereby generating four more electrons. The number of electrons and ions, therefore, increase in much

the same manner as a developing avalanche (10, p. 96). These processes can be described by the formula:

$$i = i_0 \cdot \exp\,(a_i \cdot d) \tag{2}$$

i is the electronic current reaching the anode in amps.
i_0 is the current of electrons leaving the cathode in amps.
α_i is the Townsend ionisation coefficient.
d is the length of the electrode gap in meters (9, p. 7).

The ionisation coefficient corresponds to the number of ionisation events produced by an electron in a 1 cm path along the electric field. Pictured in Figure 2 is a graphical representation of electron avalanche as caused by the Townsend mechanism.

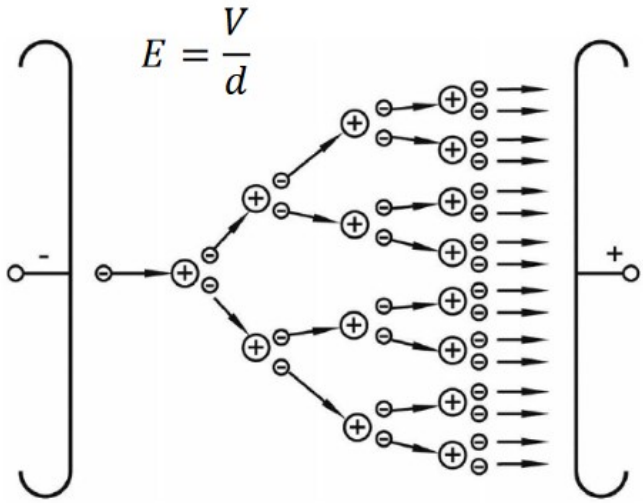

Figure 2. Visualisation of electron avalanche as caused by the Townsend mechanism. (14, p. 6).

Throughout all stages of the breakdown process electrons are constantly absorbed by the anode, thus for the Townsend mechanism to be self-sustaining, additional processes are required to produce enough starting electrons at or in the near vicinity of the cathode (9, p. 7; 14, p. 8). This is achieved by ionising UV-

radiation emitted by excited ions, as electron collisions produce not only new electrons but also bring about changes in gas molecules' electronic states (10, p. 96). Depending on gap size and surrounding pressure the UV-light may either reach the cathode directly, liberating photoelectrons at its surface, or ionise a small percentage of gas molecules in the cathode region of the primary radiation emitting volume (9, p. 8). Under the circumstances, the ionisation processes initiated by the application of an electrical field grow much like an avalanche, with a tendency to produce a self-sustained current which is almost independent from the electric field (10, p. 97).

When the abovementioned additional processes are considered, a model for the discharge current is described in the following manner:

$$i = \frac{i_0 \cdot \exp(a_i \cdot d)}{\{1 - \gamma[exp(a_i \cdot d) - 1]\}} \tag{3}$$

γ is the effective secondary emission coefficient for the cathode (9, p. 7).

It can be seen, then, that breakdown voltage depends strongly on the material of the cathode. Townsend proposed an expression which describes the parameters for initiating a self-sustaining discharge (9, p. 8):

$$\gamma[exp(a_i \cdot d) - 1] \geq 1 \; or \; a_i \cdot d \geq ln\left(\frac{1}{\gamma} + 1\right) \tag{4}$$

The Townsend mechanism is only applicable for relatively low pressures and short electrode gaps (when pressure multiplied by gap distance, $p \cdot d$, is < 200 Torr·cm) (14, p. 6). The time required for a breakdown to form when the Townsend mechanism is in effect corresponds to the travel time of an ion when crossing the electrode gap (9, p. 8). Depicted in figure 3 is a graphical summary of Townsend gas breakdown theory.

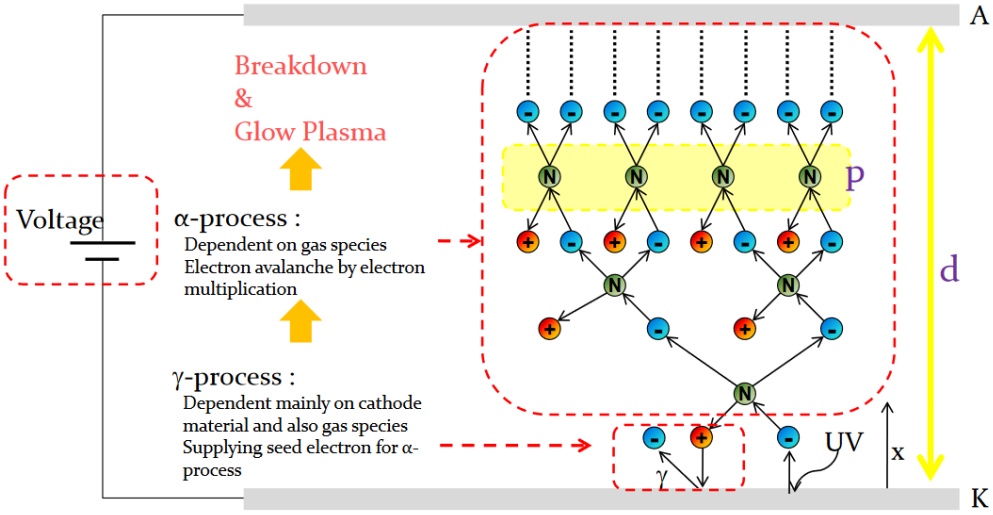

Figure 3. Summary of Townsend gas breakdown theory, where two processes, α and γ are required to sustain the discharge (14, p. 6).

2.2.3 Breakdown Models: Paschen's Law

As has been previously discussed, the electrical properties of the insulating air/fuel mixture occupying the gap between the two electrodes of the spark plug are modified with the application of high voltage, so that a conducting pathway for electrical current can be formed. Fredrich Paschen discovered empirically in 1889 the breakdown voltages of various gases between two parallel copper plates, as a function of pressure and gap distance. This can be described as follows:

$$U_B = \frac{B}{\ln\left(\frac{A \cdot p \cdot d}{ln\left(1+\frac{1}{\gamma}\right)}\right)} \cdot (p \cdot d) \tag{5}$$

U_B is breakdown voltage in volts.

d is gap distance in metres.

γ is the secondary emission coefficient for the cathode.

A is the saturation ionization in the gas at a particular electric field relative to pressure (E/p).

B is related to the excitation and ionization energies.

p is pressure in pascals.

Both A and B were determined experimentally and for air $A = 4.36 \cdot 10^4\ kV/(atm \cdot m)$ and $B = 12.8$ (11, p. 2; 12, p. 1; 15, 16). He found that for breakdown in air where the size of the gap is on the order of millimetres, an approximate estimate for the breakdown voltage is $V = 30 \cdot p \cdot d + 1.35\ kV$, where p is in atmospheres and d is in centimetres (12, p. 1).

When the abovementioned expression has been simplified with respect to the gas- and cathode-specific constants, breakdown voltage only depends on the multiplication of p by d:

$$U_B = \frac{B}{\ln\left(\frac{A \cdot p \cdot d}{ln\left(1+\frac{1}{\gamma}\right)}\right)} \cdot (p \cdot d) = f \cdot (p \cdot d) \tag{6}$$

The main factors affecting breakdown, according to the model, are therefore voltage, pressure, gap size, gas species and electrode material (14, p. 10). Bowker found experimentally that changes to the temperature (up to 860° C) and pressure of the insulating gas make no difference to the breakdown voltage as long as gas density and gap size remain constant (17, p. 110). This gives rise to the notion that within the range that Paschen's law is valid (the range within which the Townsend mechanism is most prevalent), the spark potential is a function of the mass of gas between the electrodes (as $m = \rho \cdot V$) (9, p. 9).

2.2.4 Breakdown Models: Streamer Mechanism

When large electrode gaps, high gas pressure (i.e., when the result of $p \cdot d$ is large), and high over-voltages are in use, Paschen's law is known to fail, as breakdown develops much faster than the Townsend mechanism predicts (9, p.10, 16). Over-voltage refers to a voltage which, at the moment of discharge initiation, exceeds the threshold necessary to produce a stationary glow discharge (18, p. 134). Loeb, Meek, and independently, Raether developed a new theory which described breakdown phenomena in these circumstances more accurately. Loeb and Meek developed the theory to describe the positive streamer, while Raether independently proposed a similar concept for the negative streamer (14, p. 17). According to the theory, a thin ionised channel

forms between the electrodes at a certain stage in the development of a primary electron avalanche. The main mechanism responsible for the breakdown of the electrical properties of the gas occupying the gap is photoionization: the streamer begins to form when, as a result of photoionization due to the primary avalanche, numerous secondary avalanches manifest close to the positively charged trail of the primary avalanche, and consequently the newly produced electrons are pulled into the trail (9, p. 10; 14, p. 17; 19; 20; 21). If the ignition coil in use produces high over-voltages, it is assumed that the streamer mechanism is the most prevalent breakdown mechanism in effect during the breakdown phase of the discharge event (9, p. 12).

Streamer formation is dictated by the interaction of space charge fields with the applied electric field between the two electrodes (11, p. 2; 9, p. 10). A space charge field is a local electric field that forms within the applied electric field. The avalanche becomes a dipole producing a resultant space charge field when electrons and ions are quickly distributed to opposite ends of the avalanche due to the much greater drift velocities obtained by the lighter electrons and each particle's inherent attraction to either the cathode or the anode (9, p. 10). Thus, the components of the primary electric field in front of the avalanche and behind it combine vectorially with the negatively charged head of the avalanche's dipole and its positively charged tail to create an enhanced, resultant local electric field stronger than the primary 11, p. 2; 9, p. 10). In the end, the enhanced field gives rise to stronger photoionization processes and the production of more starting electrons, leading to rapidly multiplying secondary avalanches and eventually the bridging of the gap with the formation of a conductive channel. The avalanche to streamer transformation takes place when the space charge field has increased to be comparable to the applied field. (14, p. 10, 11, p. 2). The transition from Townsend to streamer mechanism takes place when $p \cdot d$ values are in a range from 200 to 4000 Torr · cm (11, p. 2). The transition from Townsend to streamer mechanism is pictured in figure 4.

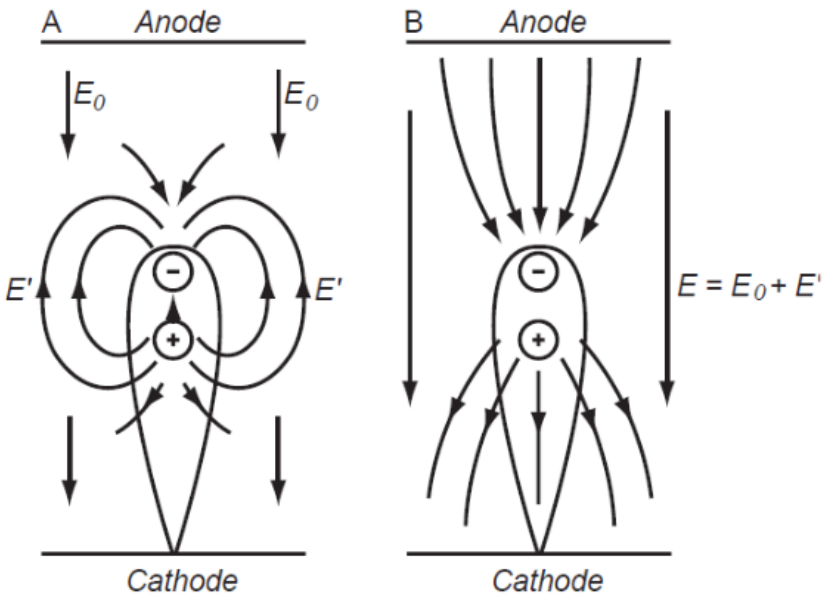

Figure 4. Townsend (avalanche) to streamer mechanism. The transition takes place when the space charge field E' is on the same order as the applied field E_0 (14)

The secondary streamer was observed as early as 1948, but not reported as a separate phenomenon until 1961 (22, p. 1358). According to research conducted in air at atmospheric pressure between a positive point and a plane, the streamer develops in two distinct phases. The secondary streamer will not form, however, if the voltage rise is sufficiently fast and voltage pulse is short (23, p. 1; 24, p. 272). During the first phase, the streamer head moves with a propagation velocity of $2 \cdot 10^5\ ms^{-1} - 2 \cdot 10^6\ ms^{-1}$ towards the cathode and develops as a small luminous zone from point anode to the plane cathode.

The first propagation of a streamer is referred to as the primary streamer. When the head of the primary streamer contacts the cathode, the second phase begins, and a so-called secondary streamer develops from the anode growing towards the cathode, forming a channel. A transient arc then forms when the secondary streamer bridges the gap (22, p. 1358; 23, p. 1; 25, p. 1952). Relatively high electric fields exist in the primary streamer's head, while the secondary streamer's electron energy is around 5-10 times lower than that of the primary streamer. The primary streamer discharge is a non-equilibrium non-thermal plasma, where the temperature of its electrons is greater than the temperature of

its ions and neutral particles ($T_e \gg T_i \gg T_n$) (24, p. 272). In figure 6 a graphic of the primary streamer-secondary streamer-spark sequence is displayed.

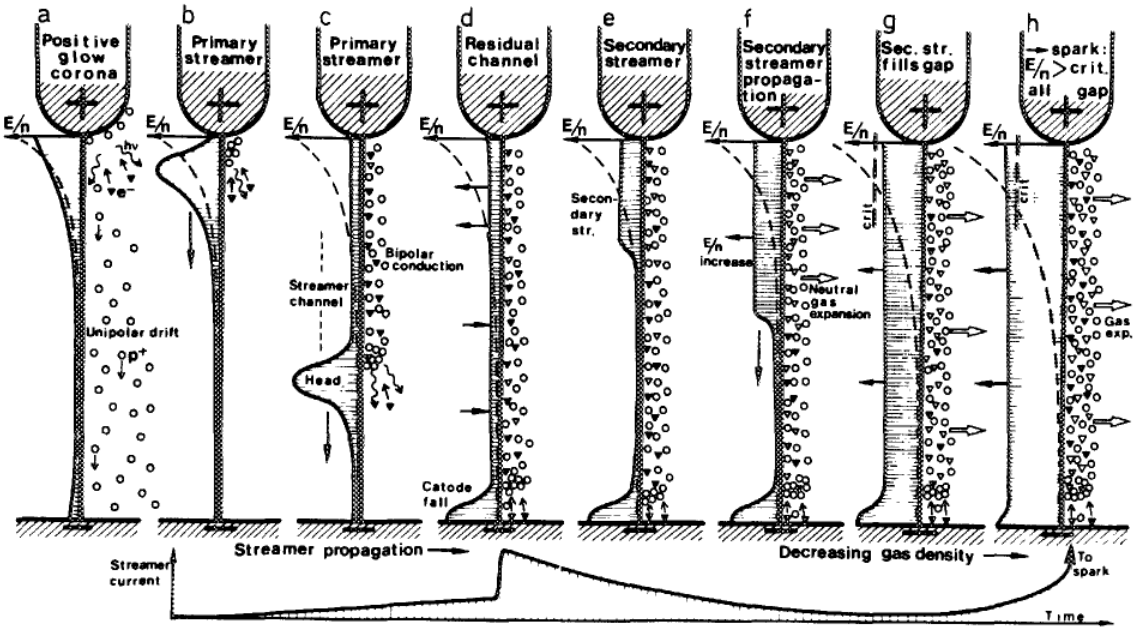

Figure 5. Drawing of the primary streamer-secondary streamer-spark sequence. (a) represents a rapidly oscillating or continuous positive point-to-plane glow corona. (b) – (c) represent the propagation and formation of a primary streamer. (d) details the formation of a residual channel, while (e) – (f) depict the formation of the secondary streamer. Stages (g) – (h) highlight the process of transition from streamer to spark when gas density has been sufficiently reduced to increase the reduced electric field above the critical value for positive net ionisation, where the secondary streamer bridges the gap as a result (22, p. 1356).

The streamer is said to be anode-directed or negative, if it grows towards both electrodes or just the anode. This is caused by large electrode gaps and high overvoltage. If the streamer propagates from the anode to the cathode, it is said to be cathode-directed or positive, which results from the use of small electrode gaps (9, p. 10-12; 14, p. 22-23). A depiction of cathode and anode directed streamers is found in figure 7.

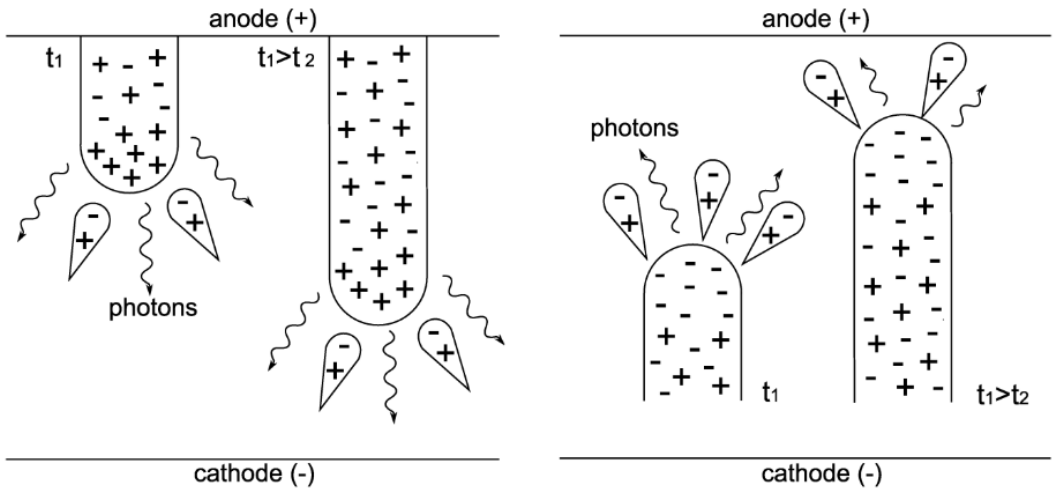

Figure 6. Visualisation of cathode directed streamer (left) and anode directed streamer (right) at two consecutive moments. Photoemission and secondary avalanches are depicted in front of the streamer head (9, p 12).

2.2.5 Arc Discharge

For an arc discharge to initiate in an insulating medium, the breakdown of the electrical properties of that medium must first take place. At the beginning of the arc discharge phase, current is that which was achieved at the moment of breakdown, on the order of >100 A (10, p. 94.) Arc current is ultimately dependent on the impedances of the external circuit, which includes spark plug leads, connectors and the spark plug itself. According to Maly and Vogel, typical values for arc discharge current are in the range of 500 mA to several kA, whilst burning voltages are relatively low (~50 V in air at 1 bar with a 1 mm gap) a result of the ionized pathway created during the breakdown phase (26, p. 822). The capacitance of the spark plug cables and secondary side of the ignition coil determine the energy fraction discharged during arc phase (≅ 70 – 150 pF) (10, p. 95). Arc energy increases quadratically with the ignition voltage according to the previously mentioned relationship,

$$E = \frac{C \cdot U^2}{2} \text{ (1, p. 156).} \quad (1)$$

For the arc to be sustained, small areas of the cathode must be heated to over 3500 K, which may be sufficient to reach the boiling point of the cathode material depending on its composition, to allow efficient emission of electrons via thermionic, field or thermo-field emission (27, p .140). The heated areas are known as cathode hot spots and the voltage drop (approximately 30 % of the burning voltage) that arises due to their occurrence provides the electromotive force required to maintain electron emission during the arc phase (9, p. 19; 10, p. 101).

By its nature, the arc discharge at atmospheric pressure or above is an equilibrium or thermal plasma; the temperature of its electrons, ions and neutral particles are almost equal ($T_e \cong T_i \cong T_n$) (27, p. 140; 29, p. 1; 30, p. 578). According to Herberlein et. al. (27, p .140), the temperature of arc plasma can be between 7000 – 25000 k, depending on arcing medium and configuration, however, as Maly (10, p. 102) comments in his study pertaining to spark ignition in the internal combustion engine, the upper and lower limits of the temperature of arc plasma in an automotive application are in the range of 5000 - 6000 K. Typically, this phase lasts around 1 µs, however, the duration may be increased to some hundreds of microseconds if arc current is above 200 mA, impedance is low and/or pressure surrounding the gap is high (9, p. 5; 10, p. 95). Ultimately a small interface on the surface of the arc plasma is responsible for the initiation of ignition, where energy transfer from the plasma core is achieved inefficiently via heat conduction and mass diffusion (9, p. 16; 10, p. 136).

2.2.6 Glow Discharge

In the case of inductive ignition systems, the glow phase is the longest and can last up to several milliseconds. Where CDI systems are concerned, the third phase of the ignition spark is also a glow phase, however, its manifestation is specifically dependent on the impedance of the external circuit. If spark current is 100 – 200 mA, rapid transitions between arc and glow phases can occur (10, p. 95). High pressure may also bring about a transition to the arc regime. Here the largest fraction of the spark’s energy is released by the energy storage device itself. For CDI it is the energy stored by the primary storage capacitor and in the

case of IDI, the inductive component remaining in the ignition coil after arc discharge (approximately 30-100 mJ) (1, p. 156; 10, p. 95).

Because the temperatures of participating particle species are not in equilibrium, glow discharge plasma is, therefore, non-thermal in nature and thus also a non-equilibrium plasma. In typical automotive ignition applications, the glow discharge is, therefore, similar to the arc discharge, except for a difference mainly in the temperature of the cathode. The degree of ionisation is low which provides the conditions for only low current densities and hence low currents. (10, p. 95; 30, p. 95). Subsequently, the effective resistance of the gap is greater during glow discharge than during arc discharge (12, p. 1). Burning voltage at 1 bar and with a 1 mm gap has been found to be ≅ 500 V and, in accordance with Paschen's law, increases with increasing gas pressure, where the size of the gap remains constant. Under these conditions, the plasma kernel temperature is 3000 K (10, p. 104-105).

2.2.7 Further Factors Affecting Formation of Ignition Spark

Several other factors significantly influence the properties and formation of the ignition spark. The spark plug's cathode, through electron emission, plays a crucial role in the process of initiating and sustaining the spark, and as such cathode material and its work function contribute greatly to the nature of discharge phases (9, p. 16). Corrigan et. al. found that the geometry of the ground electrode affects the combustion stability and breakdown voltage of spark plugs in use in Formula 1 engines designed according to the 2014 regulations (31, p. 223). Degree of electrode fouling, air/fuel mixture flow velocity and turbulence, density and composition of the air/fuel mixture have also been found to markedly affect ignition performance (1, p. 156; 8, p. 14; 12, p. 1).

2.3 Energy Transfer Efficiencies of Ignition Systems

The energy transfer efficiency of an ignition system can be defined in terms of the fraction of stored electrical energy that is transferred from the ignition system's primary storage device to the surrounding gas/plasma. Of the energy

that reaches the electrodes, some will be lost as radiation and in direct heating of the spark plug, some will be deposited in the gas but be conducted into the spark plug and surrounding combustion chamber, and some will remain in the gas (32, p. 1). Due to the use of suppression resistors for the purpose of dampening radio frequency interference (RFI) and electromagnetic interference (EMI) in spark plugs and ignition leads, in addition to ohmic resistance in the ignition coil and possible fouling of the spark plugs, significant energy is lost between the energy storage device and spark plug electrodes and is, therefore, unavailable as ignition energy (1, p. 157). According to the literature, in some cases energy available at the electrodes, as a percentage of stored electrical energy, is as low as 1 % or less, whilst more typical values for modern IDI systems are on the order of ~30–65 % (1, p. 157; 33, p. 1; 34, p. 62).

A large portion of electrical energy is dissipated as heat in the electrodes, which in turn leads to the degradation of said electrodes. Ions close to the cathode are accelerated by the intense electric field, transferring a portion of their energy upon collision as heat. This heat energy is required to sustain electron emission, however, a significant portion of it is lost through conduction to regions outside the direct area of bombardment. Energy is also dissipated at the anode when electrons are absorbed (9, p. 25). Furthermore, specific transfer efficiencies are attributed to each discharge mode earlier discussed and as such, only small portions of the electrical energy supplied to the spark plug gap may be transmitted to the air/fuel mixture for inflammation (10, p. 105).

2.3.1 Energy Transfer Efficiency During Breakdown Phase

The breakdown phase is the most efficient, with experimental results showing that over 90 % of the electrical energy is transferred to the plasma. This is due to the rapidity with which energy release occurs (in nanosecond range) and the fact that cooling processes cannot take place (9, p. 26). Extensive investigation conducted by Maly found that breakdown-phase transfer efficiencies are not affected by high flow velocities of the mixture (up to 100 m/s). Maly also found that higher energy input during the breakdown phase will result in a faster flame front speed (10, p. 115). Efficiency losses during this phase also depend on

stored energy inputs, which are caused by the emergence of a subsequent arc phase, due to the ignition system's inability to discharge all stored energy during the breakdown phase (10, p. 107). A graph of the total transferred energy vs the supplied electrical energy to the gap during breakdown discharge is displayed in figure 8. The efficiency of the discharge produced by a transistorised coil ignition (TCI) system is also shown in the figure for comparison (10, p. 106). The TCI system is a transistorised improvement of the conventional IDI system, which produces a discharge identical to that produced by the conventional IDI system (spark discharge, composed of predominantly arc and glow phases) (1, p. 148).

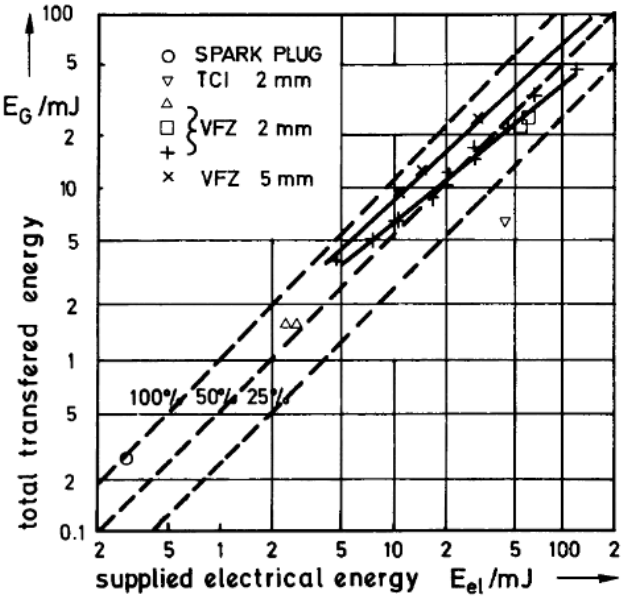

Figure 7. Energy transfer efficiency of the breakdown discharge as compared to the discharge produced by a TCI system (10, p. 106).

2.3.2 Energy Transfer Efficiency During Arc and Glow Phases

Arc and glow discharge phases are comparatively inefficient due to the formation of cathode and anode layers and heating of the electrodes. As such, electrode geometry and material also strongly influence the efficiency of these phases (9, p. 26). Teets and Sell studied the energy transfer efficiency of the glow phase and found it to be strongly dependent on gap size and gas pressure. Results indicated that efficiencies varied from 5% to 65% and that the highest efficiencies

are achieved with increased pressures and gap spacings (32, p. 1). Kim et. al. determined that the energy transfer efficiency of the arc phase also increases with increasing gap size and gas pressure, and their results ranged from 3% to 40% energy transfer efficiency for those phases (35, p. 1). Other research indicates the glow phase as the least efficient of the three, with results showing efficiencies of between 10 % and 30 % (9, p. 26). Energy available for inflammation at the plasma surface of the spark is ultimately determined by the temperature profile and geometry of the plasma, and therefore energy transfer efficiency is not a direct indication of a discharge's inflammation capability (10, p. 108). In figure 8, the energy balance for breakdown, arc and glow discharges under idealised conditions is shown.

Energy Balance for Breakdown, Arc, and Glow Discharge Plasmas under Idealised Conditions (Very Small Electrodes)

	Breakdown	Arc discharge	Glow discharge
Radiation loss	< 1 %	ca. 5 %	< 1 %
Heat conduction via electrodes	ca. 5 %	ca. 45 %	70 %
Total losses	ca. 6 %	ca. 50 %	ca. 70 %
Total plasma	ca. 94 %	ca. 50 %	ca. 30 %

Figure 8. Energy balance for breakdown, arc, and glow discharges. Adapted from [10, p. 99].

2.4 Properties of Plasma

As stated in Goebel's Fundamentals of Electric Propulsion: Ion and Hall Thrusters, plasma "is a collection of various charged particles that are free to move in response to fields they generate or fields that are applied to the collection", and more generally according to Inan and Golkowski, "plasma is any state of matter which contains enough free, charged particles for its dynamical behaviour to be dominated by electromagnetic forces" (36, p. 37; 37, p. 3). Over 99% of matter in the universe is in the plasma state, often described as the fourth state of matter. Particles making up a plasma form a system consisting of free electrons and ions; the overall charge densities of the constituent free electrons and ions cancel each other out, where $n_e \cong n_i$ (38, p. 5). As such, plasma exhibits a net neutral charge. The behaviour of a plasma is largely determined by the

Coulomb force, whereby any charge imbalance will immediately produce an electrostatic field in accordance with Gauss's law:

$$\nabla \cdot E = \frac{\rho}{\varepsilon_0} \tag{7}$$

$\nabla \cdot E$ is the divergence of the electric field.
ρ is the charge per unit volume.
ε_0 is the permittivity of the vacuum.

If the same plasma composed of a set of non-net-neutral charges were to move at velocities corresponding to v_e and v_i, a current density will arise which in turn induces a magnetic field in accordance with Ampere's law (39, p.1):

$$\nabla \times \mathrm{B} = \mu_0 \cdot J \tag{8}$$

$\nabla \times \mathrm{B}$ is infinitesimal circulation of the magnetic flux density.
μ_0 is the magnetic constant.
J is the total current density.

Most terrestrial plasmas begin as gases (40, p. 6). Plasma is formed when the gas is ionised and decomposed into negatively charged electrons and positively charged ions. Ionisation takes place when the gas is bombarded with radiation (cosmic, UV, etc.) or accelerated particles (ions, electrons, positrons), which gain their momentum under the influence of an electric field, and an amount of energy is transferred to a bound electron which is sufficient to liberate it from its interaction with the nucleus and other electrons of the gas molecule or atom (41). Importantly, a gas will behave as a plasma with a very low degree of ionization. For example, when approximately 1 % of a gas has been ionised, its electromagnetic properties will be changed such that its conductivity will be almost the same as a fully ionised gas (37, p. 4). A plot representing the classification of different species of plasma in terms of electron temperature and electron density is displayed in figure 9.

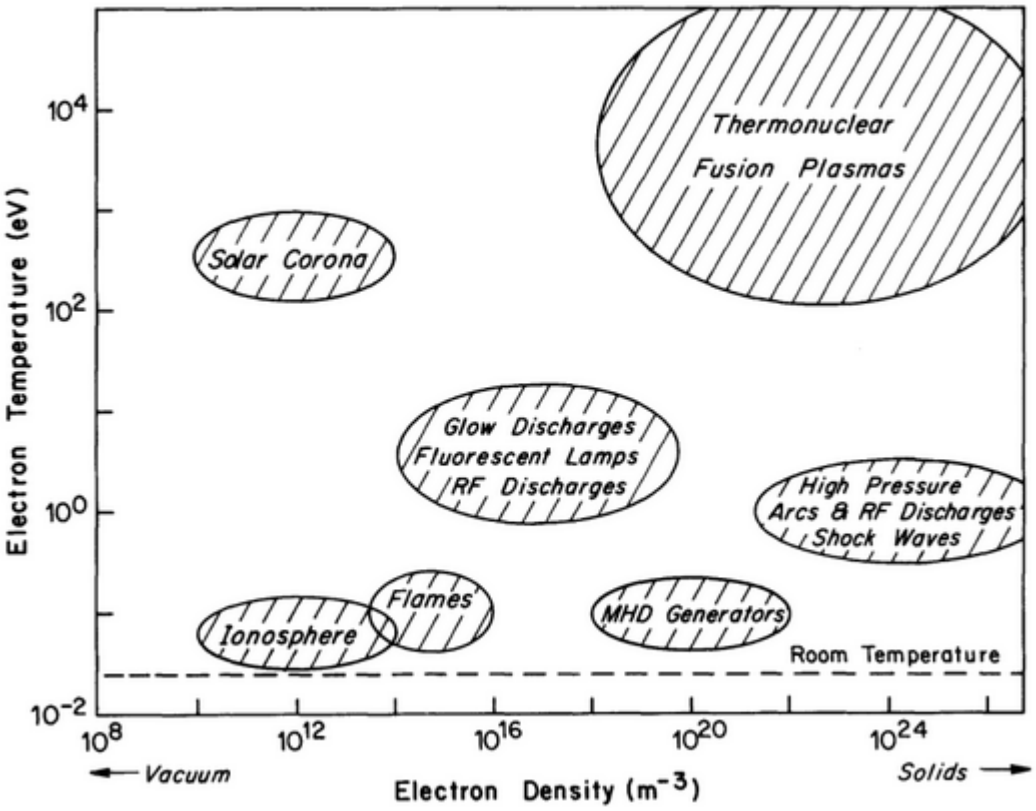

Figure 9. Classification of plasmas with respect to their electron temperature and electron density (42, p. 6).

2.4.1 Non-Thermal, Non-Equilibrium Plasma

Plasmas are commonly classified in terms of their electron temperatures. A plasma is defined as non-thermal or 'low temperature' (LTP; low-temperature plasma) when the temperature of its electrons significantly exceeds that of its ions and neutral gas molecules ($T_e \gg T_i, T_n$). As such its constituent particles are not in thermodynamic equilibrium, and accordingly, they are, therefore, also known as non-equilibrium plasmas (28, p. 1). Low-temperature plasmas are also weakly ionised, necessitating relatively low electron densities. In most cases they exist at pressures $p < 10\ kPa$ (42, p.8).

2.4.2 Thermal, Equilibrium Plasma

A thermal plasma is said to be high temperature and possessing a state of equilibrium; the temperature of its electrons, ions and neutrals are in complete local thermodynamic equilibrium (CLTE; $T_e \cong T_i \cong T_n$). Many plasmas treated as thermal plasmas are in fact only in partial thermodynamic equilibrium, however, for engineering applications deviation from CLTE is insignificant. High temperature plasmas generally occur at pressures $p > 10\ kPa$ and possess electron densities from $10^{23} - 10^{26}\ m^{-3}$ (42, p. 7).

2.5 Enhanced Ignition Systems Over the Years

Thermal equilibrium and non-thermal equilibrium plasmas have been relied upon in spark ignition systems to ignite, and stabilise the combustion of, combustible mixtures in IC engines since the first IC engine was developed by JJ Lenoir in 1858 (10, p. 110; 43, p. 1). Since then, primarily regulatory pressure based on the need to limit the environmental impact of emissions produced by IC engines has driven the development of many novel ignition systems seeking to also improve thermodynamic efficiency and fuel economy through optimisation of mixture ignition (24, p. 281; 44, p. 1690; 45, p. 1516; 46, p. 341). It is generally recognised that the operation of an SI IC engine with an air/fuel equivalence ratio greater than 1 is effective in reducing the emission of pollutants and enhancing thermal efficiency (47, p. 1, 48, p. 1). Emissions reduction strategies based, therefore, on leaner stoichiometry, such as lean burn regimes and charge stratification, place particularly heavy demand on the ignition system and especially the system's ignitor(s). To fulfil ever more extreme performance requirements many new designs have sought to enhance ignition processes and support combustion by enabling the ignition system to produce markedly different species of plasma to those produced by more conventional systems. Some of these designs and their attributes will be discussed as follows.

2.5.1 Plasma Jet Ignition System

The concept and use of the plasma jet is well established, having been introduced as early as 1957 (49, p. 80-90). Typically, the system consists of a unique ignitor and ignition circuit: the ignitor's central electrode is recessed from the surface, and that surface itself acts as the other electrode. Thus, there exists a cavity within which the spark discharge takes place. Some designs feature a discharge outlet whose diameter is smaller than that of the cavity (50, p. 3; 51, p. 1757). An example of a prototype plasma jet ignitor produced by Asik and colleagues for the Ford Motor company is found in figure 10.

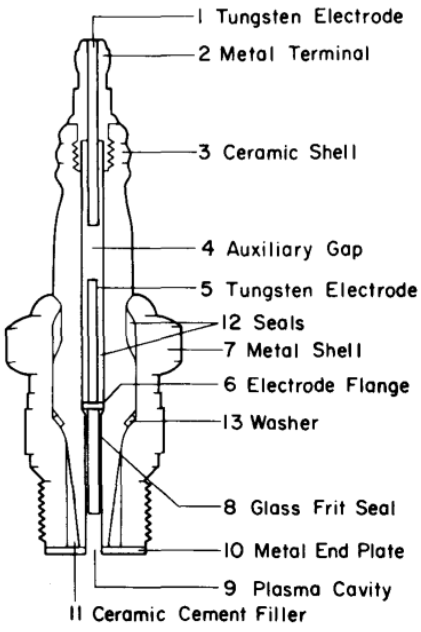

Figure 10. Sectioned drawing of a prototype plasma jet ignitor (45, p. 1517).

The air - fuel mixture is compressed into the cavity from the combustion chamber by pressure differential when the piston completes its compression stroke. A conventional inductive ignition coil is responsible for initially closing an auxiliary gap and the gap between the ignitor's electrodes by dint of the ionised pathway and electric spark it produces. The power supply is augmented by the addition of a capacitor charged to 900-1200 V, which is triggered to discharge a relatively

low voltage, high current across the gaps when the initial spark opens low resistance pathways to ground. Henceforth, high temperature plasma is created rapidly within the cavity such that it becomes pressurised, and consequently a supersonic plasma jet is issued from the discharge outlet into the charge occupying the combustion chamber (50, p. 3). A detailed visualisation of a plasma jet ignitor's discharge outlet and the development of plasma and flame kernels from said outlet is found in figure 11.

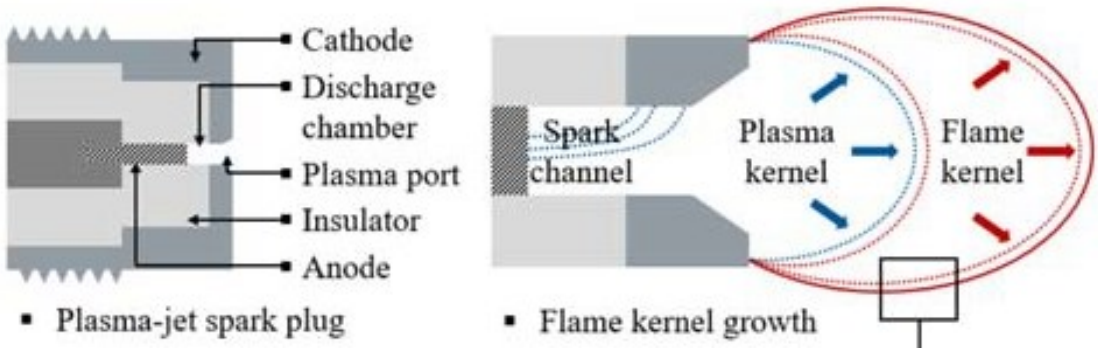

Figure 11. Schematic of a plasma jet ignitor's discharge outlet and plasma and flame kernel growth during combustion event (52, p. 835).

According to a review conducted by Dale and Oppenheim, plasma jets have been shown to be capable of igniting gaseous mixtures below the normal flammability limit (50. p. 3). Asik found that plasma jet ignition reduces both the ignition delay and burn time under lean conditions (45, p. 1528). The system requires, however, at least 1 – 2 J of energy per firing, which leads to large electrical power drain at high engine speeds and increased electrode erosion (45, p. 1528; 53, p. 783). Such erosion characteristics also indicate the presence of a predominant arc phase during the discharge, and therefore also the presence of equilibrium plasma (24, p. 269; 28, p. 1; 54, p. 25).

2.5.2 Breakdown Ignition System

Maly and Vogel determined in 1979 that not only is the increased power of the breakdown regime far more efficient at imparting energy to a gaseous environment (energy transfer efficiencies can be as high as $\approx 95\ \%$), but based

on the shape of the temperature profile across a flame front of various stoichiometric to lean methane/air mixtures, it was found that flame front velocity was also markedly increased over corresponding results obtained during arc and glow discharges (26. p. 828). Zeigler et. al. confirmed that the use of an experimental breakdown ignition system (VFZ) on a production four-cylinder engine is attributed to significantly reduced initial combustion time when compared to a conventional transistorised coil ignition (TCI) system (55, p. 1). Later Anderson (56, p. 1) came to similar conclusions when comparing the burning rate and ignitability of breakdown, capacitive discharge, conventional inductive and long duration ignition systems using premixed propane on a single cylinder engine. Pictured in figure 12 is a graphical comparison of measurements of flame growth produced by a standard IDI system and a breakdown ignition system as a function of time taken in lean turbulent conditions (57, p. 9).

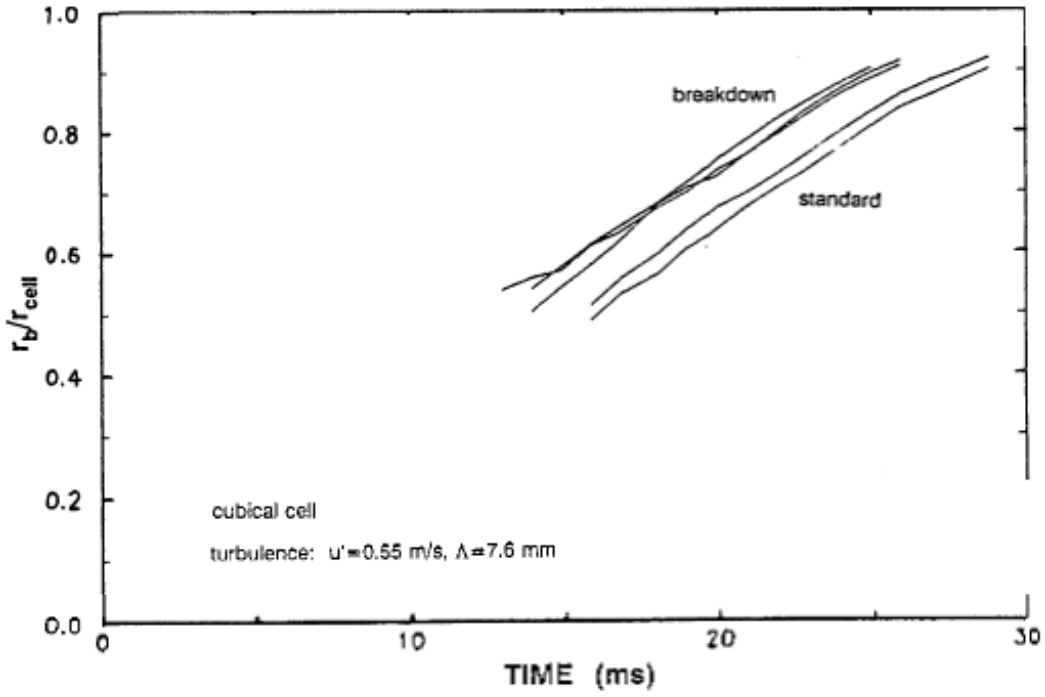

Figure 12. Graphical representation of comparison of flame growth produced by a breakdown ignition and standard IDI systems in lean turbulent conditions. Air-fuel equivalence ratio λ = 1.176, turbulence RMS intensity, u' = 0.55 m/s and turbulence integral length scale, Λ = 7.6 mm (57, p. 9).

The VFZ system tested by Anderson utilised a modified CD ignition circuit for energy supply, unmodified traditional J-gap spark plugs as ignitors. With this system, high-power input is achieved by virtue of additional capacitance coupled to the plug gap. The circuits employed by Ziegler and colleagues and Modien and colleagues also relied on additional capacitance coupled to the spark plug gap to facilitate a high-power discharge (55, p. 2; 56, p. 3; 57, p. 2). The discharge circuit's impedance must be as low as possible, therefore non-resistor spark plugs are used (55, p. 2; 56, p. 3). Depicted in figure 13 is a basic schematic of the breakdown ignition system with augmented CD ignition circuit as tested by Anderson.

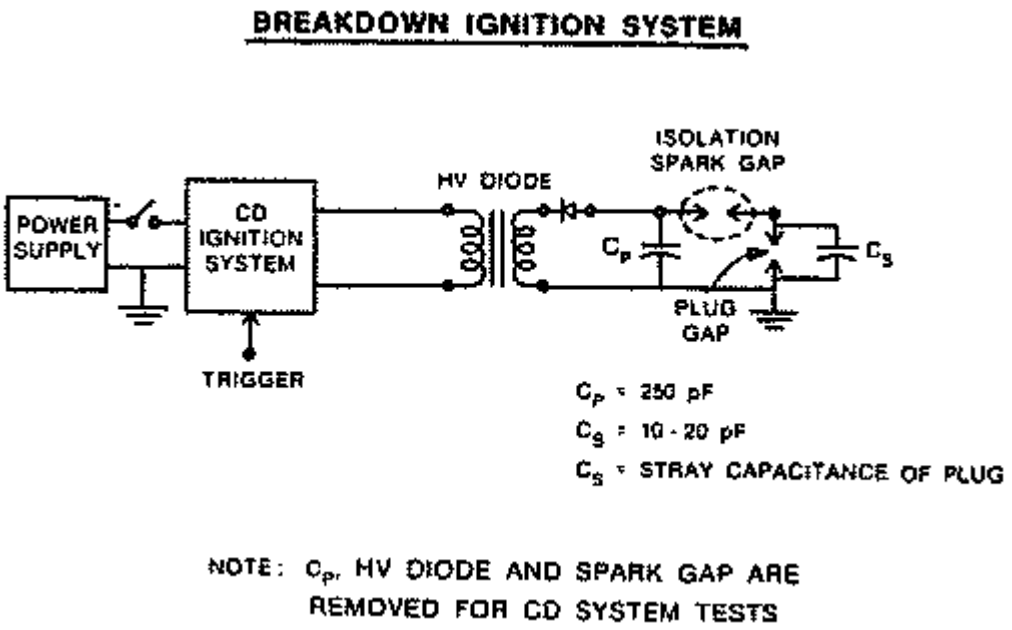

Figure 13. Schematic of Anderson's breakdown ignition system with augmented CD ignition circuit. Note the values of the capacitors C_p and C_s (56, p. 3).

According to Zeigler and colleagues (55, p. 11) the breakdown system gives better fuel consumption, lowers emissions, and extends the lean limit of operation of the engine at partial load, at idling and on overrun. This supports earlier findings made by Maly and Vogel and later Maly (10, p. 115; 26, p. 1), that a breakdown discharge can ignite extremely lean mixtures at high flow velocities with high inflammation probabilities, and that a greater energy input in the breakdown phase leads to a faster flame propagation. Furthermore, Zeigler et.

al. (55, p. 4) demonstrated that with the VFZ system, misfiring only begins with an air fuel equivalence ratio of λ = 1.5, exhaust gas temperatures are reduced, and thermal efficiency is increased. Air-fuel equivalence ratio is defined as

$$\lambda = \frac{AFR}{AFR_{stoich}} \tag{6}$$

AFR is air/fuel ratio,

AFR_{stoich} is the stoichiometric mixture for gasoline.

The stoichiometric air-fuel mixture for gasoline is about 14.7:1 (58). Figure 14 demonstrates a VFZ-system equipped production 2.3 l four-cylinder engine's superior fuel consumption as compared to that of the same engine equipped with a TCI system. This also highlights the VFZ-system equipped engine's better thermal efficiency (55, p. 4).

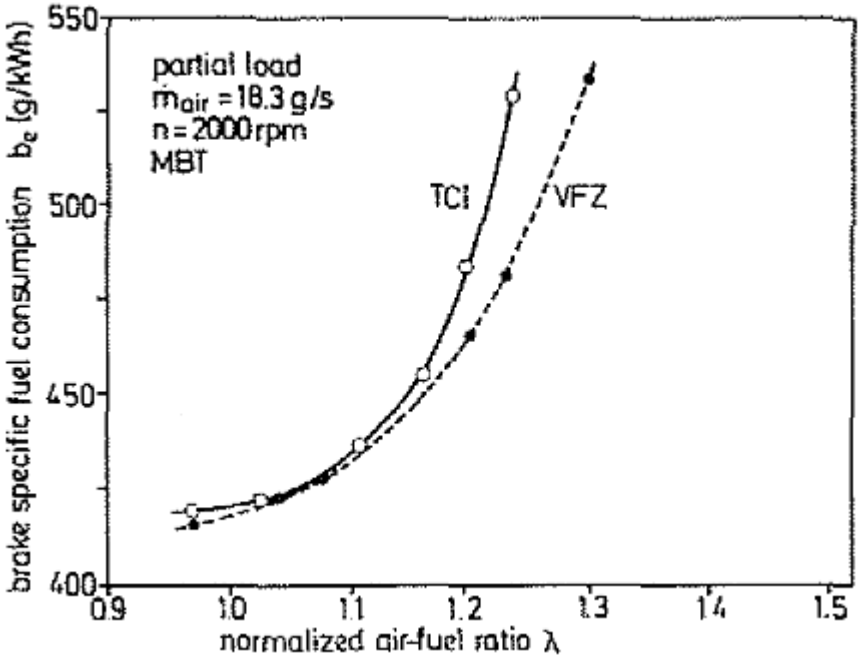

Figure 14. Brake specific fuel consumption versus air-fuel ratio for TCI and VFZ systems, engine is throttled at partial load and engine speed is 2000 rpm (55, p. 4).

It is assumed that primarily the streamer mechanism influences the characteristics of the breakdown phase of a spark discharge, due to the high

ionisation coefficient attributed to most ignition coils (9, p. 12). As the first phase of a streamer discharge is a non-equilibrium, non-thermal plasma, it can be concluded that some of the plasma influencing the breakdown ignition system's enhanced characteristics is therefore non-thermal in nature. (24, p. 272). Indeed, Starikovskaia (24, p. 283) remarks that the most valuable result of the work of Maly and Vogel, regarding different modes of the ignition spark, is that primarily combustion initiation enhancement and stabilisation occurs during the nanosecond phase (breakdown phase) of discharge development.

2.5.3 Pulsed Nanosecond Discharge Ignition System

Pulsed nanosecond discharge (PND) has been studied for almost 130 years (24, p. 278). A high voltage short duration pulse applied to a gas at atmospheric pressure and ambient temperature will produce a non-thermal, non equilibrium plasma that is governed by the streamer mechanism, if the pulse-width is on the order of several to tens of ns. Longer pulse-widths on the order of tens to hundreds of ns can produce a thermal, equilibrium plasma in the form of an arc (24, p. 278). When the over-voltage at the initiation of discharge is tens of percent, the breakdown will transform from a uniform glow propagated by the Townsend mechanism into a streamer breakdown. If the over-voltage is considerably greater (≥ hundreds of percent), the breakdown will become spatially uniform (24, p. 279). This high over-voltage pulsed nanosecond discharge takes the form of a fast ionisation wave (18, p. 134). One of the major advantages of using a spatially uniform non-thermal plasma discharge to initiate combustion is that it can bring about the formation of multiple flame kernels over a wide area at a low level of energy consumption (59, p. 2).

Modern electronics have made the generation of highly repeatable (frequencies of up to tens of kHz) spatially uniform discharges possible (24, p. 278-279). Typically, voltage rise times are very short ($\geq 1kV\ ns^{-1}$) and pulse amplitudes are tens – hundreds of kV with durations of 10 – 100 ns. Propagation velocity of the discharge has been noted to be high ($10^9 - 10^{10}\ cms^{-1}$) (18, p. 134). In figure 15, the development of a nanosecond discharge in air can be seen over a 12 ns period.

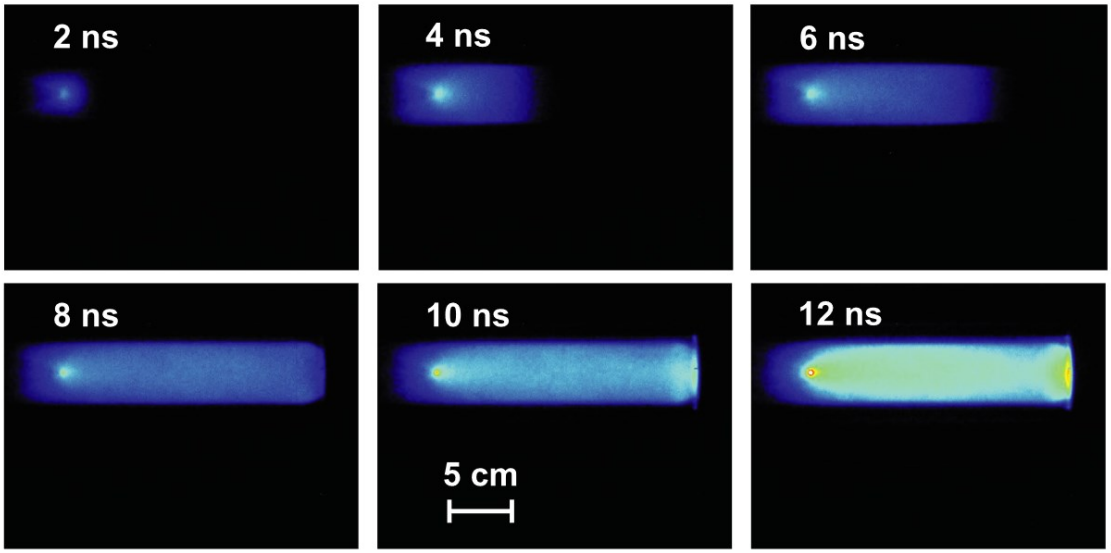

Figure 15. Successive images of the development of a nanosecond discharge in air. High voltage electrode is on the left-hand side (24, p. 280).

PND ignition systems have been tested successfully on internal combustion engines, where indicated mean effective pressure (IMEP) and pressure at the moment of ignition are much greater than atmospheric pressure (59, 60, 61). The authors of [60, 61] employed an ignition circuit consisting of a high voltage pulse generator, solid core spark plug wire, and a custom spark plug. The authors of [59] also utilised a custom spark plug very similar in design; in each case the cylindrical ground electrode formed a radial gap with the central electrode. In the case of papers [60, 61], the ground electrode had four evenly spaced sections cut out, spaced 2.5 mm radially from the central electrode, while the central electrode itself was recessed from the face of the four ground electrode poles. The purpose of this design is to improve flame propagation characteristics and produce a pronounced reduced electric field (62, p. 2; 60, p. 2). The authors of [59] experimented with a threaded central electrode, which led to improved uniformity of streamer formation in the circumferential direction of the cylindrical ground electrode (59, p. 2). In figure 16 the differences in electrode configuration between a conventional spark plug and a low-energy transient plasma spark plug as compared by the authors of [60] can be seen.

Figure 16. Conventional spark plug (left) and low-energy transient plasma spark plug (right) (60, p. 2).

It has been found that the discharge characteristics produced by PND ignition increase the speed of combustion and improve the stability of lean operation. Sevik and colleagues (60, p. 1) tested a PND system on a gasoline direct injection (GDI) single-cylinder research engine possessing specifications representative of commercially available units (four-valve cylinder head, 40deg pentroof combustion chamber fitted with centrally mounted spark plug and fuel injector, compression ratio 12.1:1). They compared the lean and exhaust gas recirculation-dilute (EGR-dilute) tolerance of such a configuration to the performance of the same engine equipped with a conventional transistorised coil ignition (TCI) system. It was concluded that the PND system allowed for the extension of the lean limit from λ = 1.5 to λ = 1.7 and an increase of EGR by up to 20 %. Shirashi et. al. (59, p. 1) conducted a similar investigation with a custom PND ignition system installed on a four-valve, single-cylinder test engine also with a pentroof combustion chamber and concluded that such a system can produce

volumetric streamer discharges at pressures of up to 1400 kPa at an energy consumption of 60 mJ/cycle, where the initial combustion period is shortened as compared to conventional spark ignition. In figure 17 on the left, streamers generated by 56 kV, 54 ns pulse in air are displayed. Here the energy delivered by the pulse was 370 mJ, and the maximum E/n was 400 Td. On the right of figure 17, flame propagation from the base of the streamers seen on the left of the figure is exhibited, where a single pulse has been fired in a mix of C_2H_4 and air.

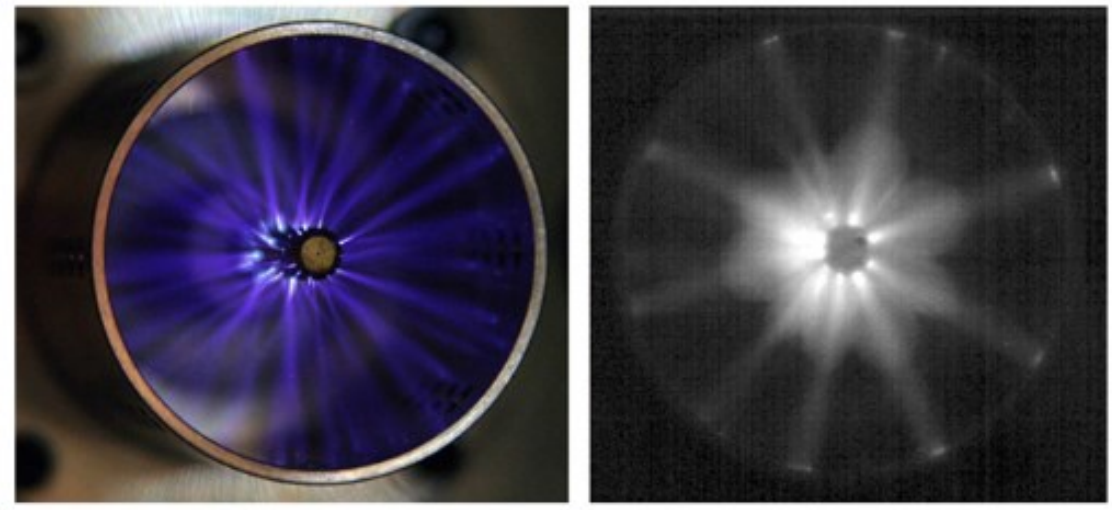

Figure 17. PND generated streamers (left) and flame propagation from a single 370 mJ, 56 kV, 54 ns pulse in a mix of C_2H_4 and air (right) Multiple ignition sites can be seen in the image on the right (62, p. 3).

2.6 Plasma Properties of Enhanced Ignition Systems

Many fundamental questions regarding the way a plasma interacts with a fuel, such as how the kinetic pathway of plasma assisted combustion is dependent on plasma properties, temperature, and fuel, are still the subjects of intense research (54, p. 25; 62, p. 1). In general, however, it has been noted that research in the field of combustion science for automotive applications has largely eschewed the development of ignition systems that produce thermal equilibrium plasmas, that is plasmas with electron energies in equilibrium with the bulk gas energy, such as conventional IDI systems (63, p 170, 54, p. 24). On the other hand, much effort has been focussed on the development of systems that produce low-

temperature, non-equilibrium plasma, whose electron and ion temperatures exist in a state of imbalance (63, p 170).

It is important to note, however, that different plasmas interact with combustion in different ways. According to Ju et. al. (54, p. 25), combustion is affected mainly by dint of three different pathways: thermal, kinetic, and transport (including aerodynamic). When the thermal enhancement pathway predominates, plasma increases temperature, and, by virtue of Arrhenius' law, which describes an exponential dependence of the rate of chemical reactions on absolute temperature, accelerates chemical reactions and fuel oxidation (64). When the kinetic pathway is in effect, plasma produces high energy electrons and ions, which further produce active radicals (such as O, OH and H) due to direct electron impact disassociation, ion impact and recombination disassociation, and collisional dissociations of reactants with electronically excited and vibrationally excited molecules. When plasma enhances combustion via the transport pathway, large fuel molecules can be broken down to small fuel fragments, which influences fuel diffusivity and therefore also the combustion process. Additionally, plasma can produce long-lifetime reactive (for example, ozone (O_3)) and catalytic intermediate species (for example nitric oxide (NO)) which can accelerate fuel oxidation at low temperatures. More specific features of the way thermal and non-thermal plasmas behave in experimental ignition systems and affect combustion and ignition will be discussed below. The major enhancement pathways of plasma assisted combustion are exhibited in figure 18.

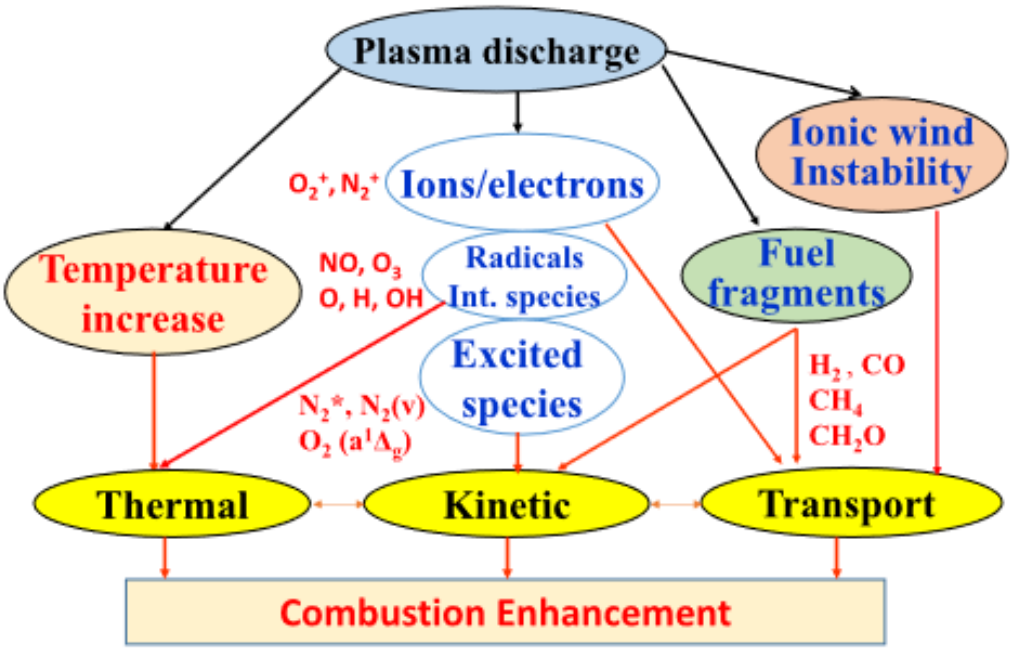

Figure 18. Major enhancement pathways of plasma assisted combustion (54, p. 25).

2.7 Plasma-Assisted Ignition and Combustion: Equilibrium Plasma

Much research has been conducted to determine the viability of automotive ignition systems that produce a high energy discharge. It is known that the ignition limit can be affected by using spark systems with increased energy and that higher spark energy can be beneficial to early flame growth positively affecting ignition characteristics (65, p. 381). This can also improve tolerance to high rates of exhaust gas recirculation (EGR) used to reduce NO_x emissions (10, p.115; 65, p. 381; 66, p. 844). In addition, the main factor that contributes to a reduction in the ignition-delay time is local heating of gas, leading to an increase in the rate of thermal dissociation (67, p. 1182). Research pertaining to these characteristics has led to the development of ignition systems such as the plasma-jet ignition system previously mentioned. In figure 19, a plot of spark timing with respect to fuel air equivalence ratio is shown, where ignition limit and partial burn lines have been overlayed on the plot to delineate areas of stable combustion, misfire,

misfire or partial burn and partial burn in terms of fuel air equivalence and spark timing.

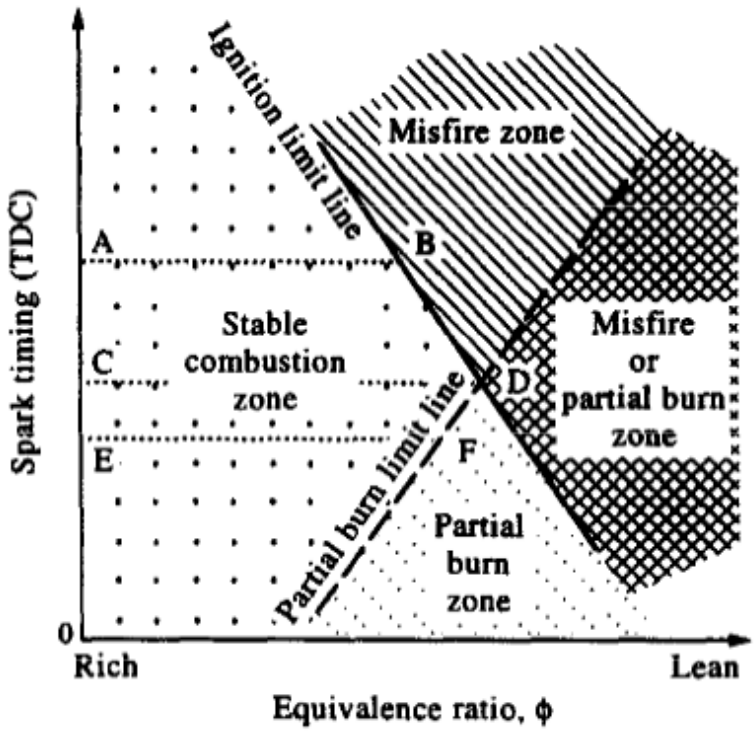

Figure 19. Zones of stable and unstable operation in lean mixtures. Ignition systems with increased energy can affect the ignition limit and promote early flame growth, thus also affecting the partial burn limit (65, p. 381).

Whilst it can be inferred that most plasma-jet ignition systems have not been designed from the outset to specifically produce thermal equilibrium plasma, the results of studies by Asik et. al and Smy et. al (45, p. 1526; 53, p. 789-790) suggest that the predominant mode of discharge produced by these systems is indeed equilibrium in nature. Smy et. al. found that the rates of erosion of tungsten, mild steel and hardened steel electrodes in a typical plasma jet ignitor were comparable to previous measurements of arc erosion, where mass erosion rates of 10^{-5} – 10^{-4} g/C were empirically demonstrated in connection with the arc discharge. The results of Smy and colleagues are not incongruent with this (53, p. 783), for the authors' published figures were on the same order of magnitude (up to $2 \cdot 10^2$ µg/C), leading to electrode lifetimes of < 10 hours. As such, it can

be inferred that the discharge consists of a prominent, high temperature, thermal plasma producing arc phase, which is dependent on cathode hot spots and the resulting emission of electrons and evaporation of cathode material to sustain the arc (10, p. 101).

In terms of combustion enhancement, thermal plasma relies primarily on the thermal enhancement pathway to influence combustion. As has been previously mentioned, the temperature of the column of the arc discharge is typically very high (7000 K – 25,000 K), which results in high energy consumption, poor energy transfer efficiency of the ignition system and ultimately poor thermodynamic efficiency of the internal combustion engine, due to excessive heat production (27, p .140; 59, p. 2). Moreover, the cost of ensuring the reliability of a mass-produced, high-energy, thermal-plasma-producing system is likely to also be prohibitive. Expensive refractory metals with high boiling points (such as iridium and wolfram) are required to ensure that erosion rates are kept to a minimum, however, the literature suggests igniter durability is always diminished when compared to that of other, non-plasma-jet ignitors of the same material (27, p .140; 48, p. 1; 63, p. 170).

2.7.1 Plasma-Assisted Ignition and Combustion: Non-Equilibrium Plasma

Improving the efficiency of plasma-assisted ignition and combustion systems (PAI, PAC), which are capable of operating in a wide range of equivalence ratios, pressures, and flow velocities, has motivated research directed at exploring the potential of low-temperature non-equilibrium plasma in ignition system-based applications (68, p. 1). Non-equilibrium plasma offers many fundamental advantages: during the earliest stages of discharge the temperature of the neutral gas and electron density are relatively low. On the other hand, electronic, vibrational, and rotational temperatures are non-uniform, and the electron temperature is high (1 – 100 eV). Consequently, high energy electrons collide with molecules and atoms, increasing their internal degrees of freedom and as such, their internal energy. This in turn gives rise to the creation of highly reactive radicals that promote oxidation chain reactions (43, p. 6; 54, p. 24).

One of the most important radical species is atomic oxygen (O), due to its ability to increase mixture reactivity because of its influence on hydrogen abstraction from the fuel (63, p 170). Kosarev and colleagues (69, p. 4) investigated the kinetic mechanism of plasma-assisted ignition of various hydrocarbons, where test samples ranging from CH_4- to C_5H_{15}- containing mixtures were ignited with a high-voltage nanosecond discharge. Results indicated that the significant decrease in ignition delay time (more than an order of magnitude) observed was due to an increase in the density of O atoms, because of electron impact dissociation of O_2 molecules in the discharge phase. Consequently, the rates of chain chemical reactions increased. Quantitative diagnostics have also been performed to determine absolute atomic O concentration and the rates of its decay in nanosecond discharges (NSD), revealing the significance of the radical as one of the main pathways for combustion enhancement (70, 929–936).

According to Starikovskaia, the dissociation rate of molecular oxygen by gas discharge, where reactions of dissociation are triggered by electron impact, is at least a few orders of magnitude greater than the constant rate for the reaction of thermal dissociation at gas temperatures typical for combustion. This is due to the creation of new reaction pathways that lead to the production of radicals more rapidly than what the fuel oxidation chemistry would normally allow. Thus, at low temperature, the kinetic pathway of enhancement can effectively lower the activation energy of the global fuel oxidation. The use of the internal energy of the atoms and molecules, therefore, can be a more efficient way to initiate a chemical transformation than by use of thermal energy alone (43, p. 6; 54, p. 26). This agrees with the kinetic modelling calculations of Adamovich and colleagues, who found that the predicted ignition delay time attributed to an NSD in ethylene-air flows was reduced by two orders of magnitude and ignition temperature by 300 K, compared to ignition by equilibrium plasma, due to the generation of chain reactions of radicals (68, p. 1).

Many different discharges are used to produce non-equilibrium plasma for the purpose of PAC/PAI, such as gliding arc discharge, microwave induced discharge, dielectric barrier discharge (DBD), RF induced discharge and PND (54, p. 24; 24, p. 278–281). Of these, PND has been found to produce the

strongest reduced electric fields, on the order of 100-1000 Td, leading to increased rates of ionisation, dissociation and production of combustion enhancing chemical radicals such as atomic O (72, p. 2; 63, p. 170). Dissociation and excitation rates of the gas occur, therefore, at a shorter time scale than that which is typical of combustion kinetics (43, p. 4; 54, p. 26). Also, plasmas produced by these discharges are more stable at high pressures compared to other electric discharges, and in the case of a multi-streamer configuration at high gas densities, are naturally synchronised in time (43, p. 4; 68, p. 2). Perhaps for these reasons, the performance of PND and NSD-based ignition systems have been investigated in several recent studies [59, 60, 61, 62, 71] concerning the viability of PAC/PAI in automotive ICE-based applications.

PND ignition systems have been found to also produce equilibrium plasma (i.e., thermal plasma) as a result of the secondary streamer breakdown (SSB) mechanism (61, p. 1791–1792). SSB occurs because of high gas conductivity, which can be attributed to high temperature, low pressure, short electrode gap distances or low gas ionisation potential, and leads to the formation of thermal, equilibrium plasma, and ultimately leads to significantly increased electrode erosion rates (63, p.170). Ikoto and Wolk investigated the probability of SSB occurrence during pulsed nanosecond discharge, depending on electrode distance, gas pressure and pulse dwell time. Their findings demonstrated that where pulse dwell times were short, the probability of SSB increased with every subsequent pulse, and that the main mechanism responsible for this increase is thermal preconditioning from the preceding non-equilibrium plasma producing pulse, giving rise to reduced electrical resistance in the gas (63, p. 186).

3 Experimental

3.1 Experimental Background

Despite the many advantages of PAI/PAC, systems for automotive applications with IC engines have not reached mass production. A multitude of patents for various technologies exist; the focus of this experimental work is to characterise the discharge produced by and evaluate the performance of a plasma ignition

circuit based on a reference circuit that has been adapted from an existing patent. This will be carried out by constructing a replica of said circuit. Circuit dynamics will be measured where possible and its nature will be assessed based on the measurements taken.

Patent US8555867B2 (73) describes a method for producing plasma ionisation by virtue of a single power circuit. According to the patent, the circuit produces a better spark by delivering to the spark plug gap, just after the formation of a spark, the energy stored in a capacitor. This is achieved with help of a one-way current path between the primary and secondary windings of an ignition coil or high voltage transformer (73). The spark produced by the circuit is said to ultimately be both high voltage and high current in nature. It is asserted that this is due to the following factors:

- The initial high voltage spark produced by the output of the secondary winding of the ignition coil.
- The low resistance path to ground across the gap after formation of the spark that gives rise to high current when the capacitor's remaining energy can dissipate through it (73).

It is also claimed that the circuit more efficiently delivers energy to the gap, because the capacitor's stored energy is not dissipated exclusively through the windings of the high voltage transformer (73). Furthermore, the authors of the patent state that the high current component of the discharge is responsible for the ionisation of air around the gap, thus leading to plasma generation (73). These statements will be evaluated in the present study. The circuit as it appears in the patent is pictured in figure 19.

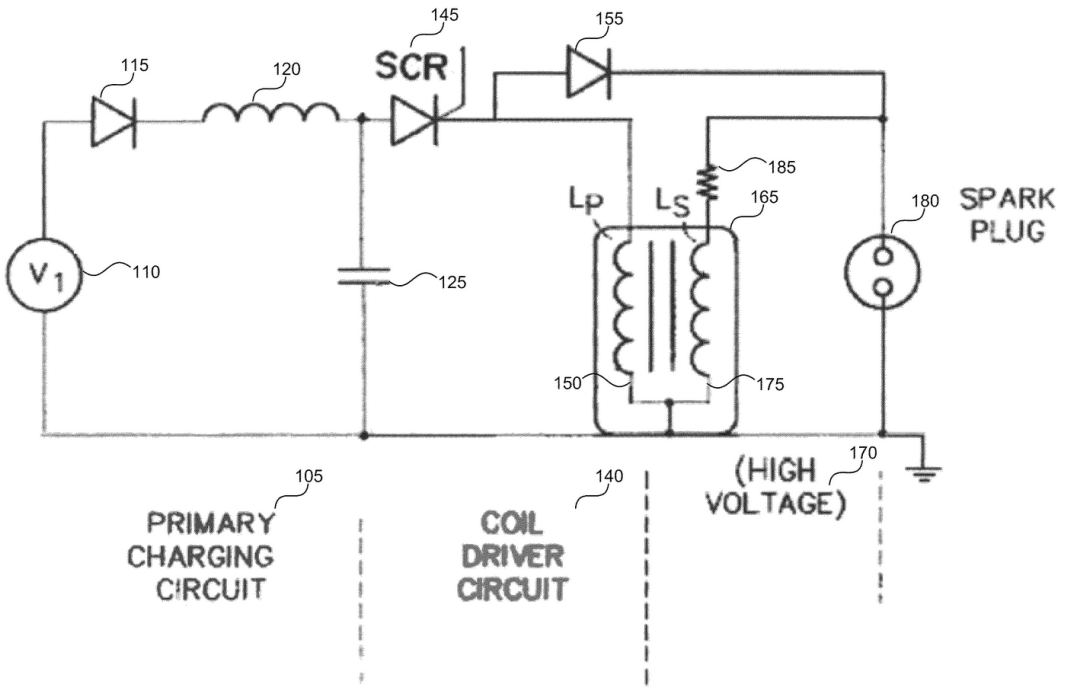

Figure 20. Circuit described in US patent US8555867B2 (73).

3.2 Methods

3.2.1 System Description

The basic circuit found in the patent (73) was replicated according to an adaptation made by Peter Lindeman (74). As in the patent, the complete circuit consisted of three sub-circuits: a coil driver circuit, a charging circuit, and an ignition circuit. Triggering of the discharges was implemented by a 555 timer-based coil driver circuit, fitted with a 1 M Ω potentiometer and a power relay, as opposed to a silicon-controlled rectifier. The frequency of the discharges could thus be adjusted via the potentiometer from approximately 1 – 15 Hz. A red indicator LED's operation was synchronised with the firing of the ignition circuit, to indicate to the user when the ignition circuit was firing. The power relay was an Omron LY2 DC12 double pole-double throw type (DPDT), with a dielectric strength between the relay coil and contacts of 2000 VAC. The relay's rated maximum contact voltage is 250 VAC and 125 VDC and its rated maximum contact current is 10 A (75). A DPDT relay configuration is composed of two switches that are operated simultaneously by the same relay coil. In this

application, it allows the charging circuit and the ignition circuit to be completely isolated from each other, where the discharge capacitor is switched to either the charging circuit or the ignition circuit. 12 VDC was supplied to the power relay through the coil driver circuit with either a TEKLAB TL303 or a TTi EX355R power supply.

Two different aluminium radial electrolytic type capacitors were used in the charging circuit: a 47 µF 350 VDC unit and a 56 µF 400 VDC unit. The charging of the capacitors was implemented in the following manner: mains ~230 VAC electricity was first regulated through a Hossoni SV 2A variable transformer capable of outputting 0-250 VAC. This was fed through a 100 Ω 20 W resistor to a full-wave bridge rectifier, and its rectified output was then switched onto the capacitor according to the relay's state. Measurements indicated the maximum output from the full-wave bridge rectifier was approximately 380 VDC.

A 12 V Biltema 1880 ignition coil was used as the circuit's high voltage transformer in the ignition circuit with a primary winding resistance of 1.2 Ω and a secondary winding resistance of 9.9 kΩ. In addition to this, a Shexton PRHVP2A-20 high voltage rectifier diode was used to facilitate the one-way current path between the ignition coil's primary and secondary windings. The diode was chosen due to its ability to handle both high voltages and high currents. An NGK-BP5ES resistorless sparkplug with nickel-alloy electrodes was used to form the spark gap over which the output from the ignition coil and discharge capacitor were discharged. The complete circuit was constructed in a modular fashion, so that components could easily be replaced or temporarily removed: provision was made for the rectifier diode to be added or removed from the circuit. When removed, the discharge capacitor would only discharge through the primary windings of the ignition coil, thus producing a discharge at the spark plug gap very similar in nature to the discharge produced by a typical commercially available CDI system. As in a typical CDI system, in this configuration high voltage is induced in the secondary windings of the ignition coil when the capacitor discharges into the ignition coil's primary windings. This feature also promoted straightforward comparative analysis of the two discharge types that can be described as follows: enhanced plasma-type and normal CDI-type. A

schematic of the complete circuit is depicted in figure 20. The constructed circuit is displayed in figure 21.

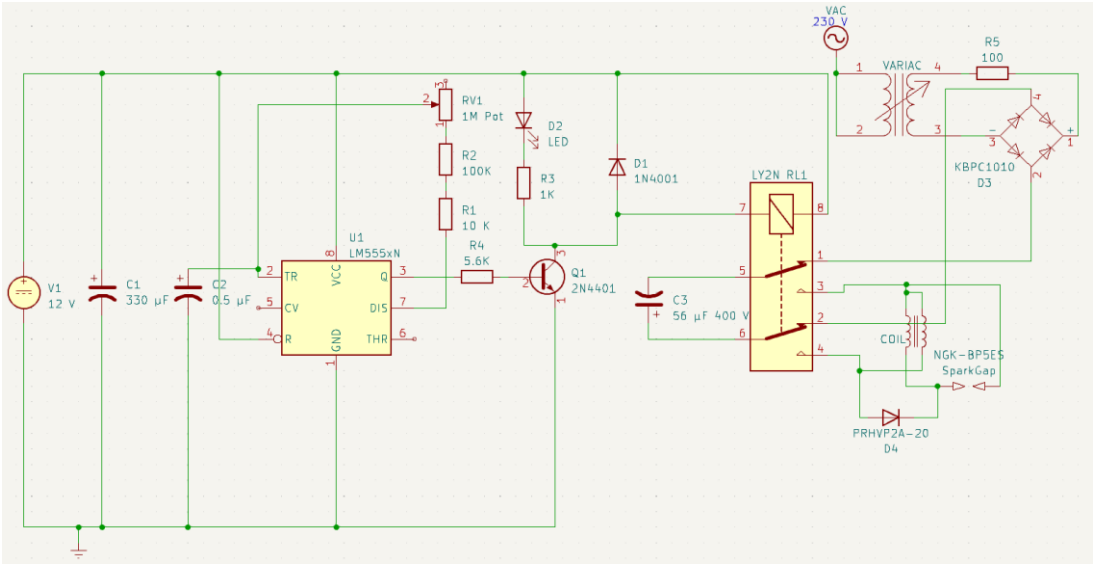

Figure 21. Schematic of the replicated adaptation of the circuit found in patent US8555867B2 (73).

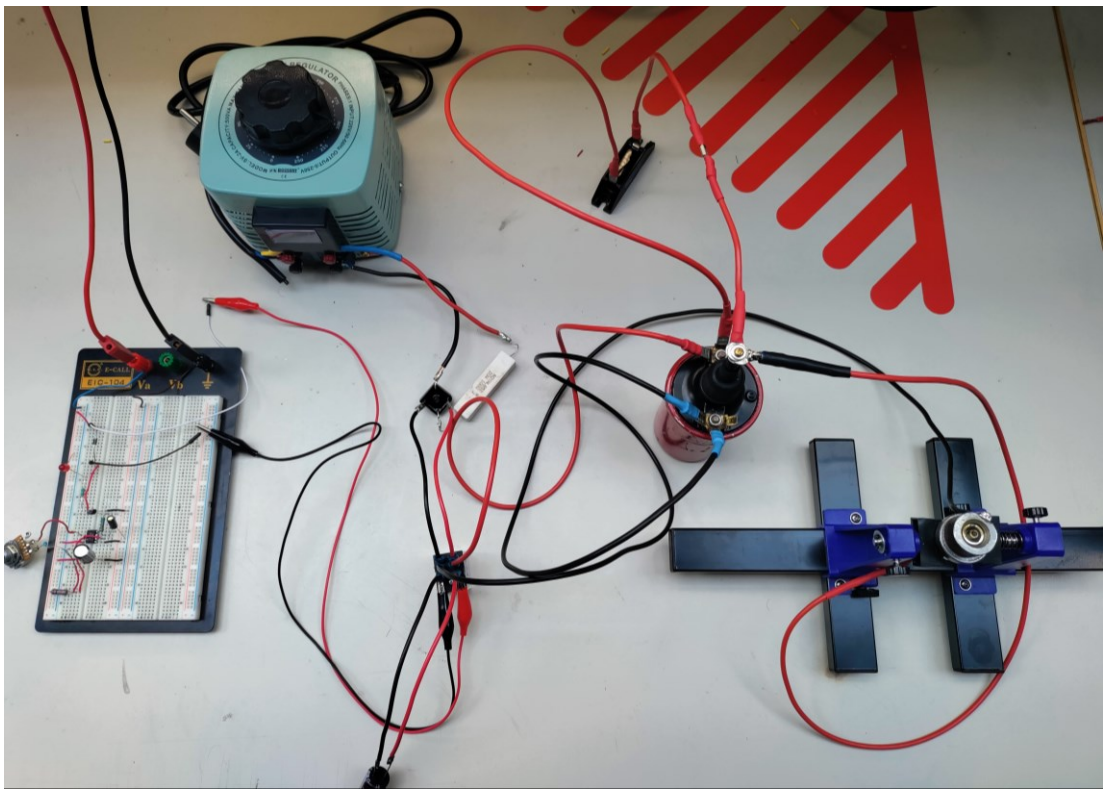

Figure 22. Constructed replication of Peter Lindeman's (74) adaptation of the circuit found in patent US8555867B2 (73).

3.2.2 Measurement Procedure: Electrical Characteristics of Different Discharges

Measuring the high voltage output of the secondary windings of the ignition coil and discharge characteristics of the 47 µF 350 VDC discharge capacitor was performed with a Pico Technology MI074 inductive capacitance probe connected to a Picoscope TA010 20:1 attenuator and Picoscope 4423 automotive oscilloscope. The oscilloscope was interfaced with a laptop running Picoscope 6 Automotive PC oscilloscope software enabling data acquisition and signal processing of the measurements. These measurements and discharge characteristics were obtained both with the rectifier diode removed from the ignition circuit and with it remaining in place, i.e., where the discharge at the spark gap was either the normal CDI-type or the enhanced plasma-type. The gap at the spark plug was set to 2.5 mm and the discharges were triggered in air at local atmospheric pressure (1010.75 mbar) and temperature (293.35 K). The discharge capacitor was charged to 314.7 VDC and the potentiometer was adjusted so that the firing frequency was 1 Hz.

Firstly, the traces of voltage output with respect to time as measured from the output of the ignition coil's secondary windings were recorded to hard disk for the 17 CDI-type discharges and 6 plasma-type discharges. The plots were then analysed and, where available, were compared to reference plots found in the literature, with a view to identifying typical features. The average rise time to the maximum measured positive value for the series of discharges, the average peak positive voltage, the average peak negative voltage, and the average rate of change of positive voltage during rise time were calculated based on the plots for both discharge types. For the CDI-type discharge, the average duration of the assumed breakdown, arc and/or glow phases were also calculated. For the plasma type discharge, the average time for the assumed complete discharge event was calculated, in addition to the average peak positive voltage increase and average peak negative voltage decrease as a percentage over the CDI-type discharge. Discharge energy before losses for these measurements, for both CDI and plasma discharge types, was therefore 2.33 J.

Following this, the traces of voltage with respect to time as measured from the discharge capacitor's terminals were also recorded to a hard disk. The plots were then analysed. The capacitor's discharge current and discharge power were calculated for both CDI and plasma discharge types based on the plots. This was achieved by determining the length of a time interval from when the measured voltage across the capacitor was 314.7 V, to when this value had decreased to 150 V. During this interval the voltage was assumed to decrease linearly. When the rate of voltage discharge $\frac{dv_c(t)}{dt}$ had been calculated for the measured time interval, the discharge current was calculated according to the following formula:

$$i_c(t) = C\frac{dv_c(t)}{dt} \tag{3}$$

$i_c(t)$ is capacitor current with respect time in amps.
C is capacitance in farads.
v_c is capacitor voltage with respect to time in volts.

The discharge power was then calculated according to the formula:

$$P_c(t) = v_c(t) \cdot i_c(t) \tag{4}$$

$P_c(t)$ is capacitor power with respect to time in watts.

Figure 22 portrays part of the measurement procedure performed when measuring the output voltage of the secondary side of the Biltema 1880 ignition coil used in the replicated circuit.

Figure 23. Pico Technology MI074 inductive capacitance probe connected to the secondary side output of the Biltema 1880 ignition coil.

3.2.3 Measurement Procedure: Characterisation of Discharge Plasma

The objective of this part of the measurement procedure was to analyse and compare the behaviour of the discharges to examples found in the literature. Characteristics typical of thermal and non-thermal plasma were of particular interest. A preliminary analysis was carried out firstly by visual and auditory assessment and photographs, where possible, were taken with a OnePlus 64 MP embedded smartphone camera. All discharges were triggered in air at local atmospheric pressure (1010.75 mbar).

After this, electrode wear rates were investigated by producing discharges across the gap according to different circuit parameters for the two discharge modes. The electrodes of the spark plugs used in the investigation were then inspected with a ZEISS Stemi 508 stereo microscope and ZEISS ZEN core 3.1 data acquisition software installed on a computer to determine the existence of certain typical features, such as evidence of cathode hot spots. The same parameter

sets were applied to both discharge modes for the investigation. Testing parameters are outlined in figure 24.

Firing mode	Spark plug gap (mm)	Measured AC voltage (V)	Measured voltage at capacitor (VDC)	Capacitor's capacitance/voltage (μF/VDC)	Firing frequency (Hz)	Total firing time (hrs:mins:sec)	Temp. start (K)	Temp. end (K)
Plasma	1	249.1	354	56/400	2.024	01:00:00	298.15	299.15
CDI	1	250.5	357	56/400	2.024	01:00:00	295.15	295.15
Plasma	1	142.5	200.2	56/400	1	00:00:01	296.15	296.75
CDI	1	142.4	199.5	56/400	1	00:00:01	296.15	296.15
Plasma	2	142.7	200.0	56/400	1	00:00:03	296.15	297.15

Figure 24. Test parameters used to investigate electrode wear rates.

3.3 Results

3.3.1 Electrical Characteristics of Different Discharges: High Voltage Output of Ignition Coil with CDI-Type Discharge

Figure 25 depicts a typical trace of voltage with respect to time produced by the output of the ignition coil's secondary windings when the rectifier diode has been removed, i.e., when the discharge at the spark gap is of the CDI-type. As can be seen in figure 26, the calculated average voltage rise time to the maximum measured positive value for the series of 17 discharges was 15.063 μs, and the average rate of change during this rise time was 9.3 kV/μs, several orders of magnitude greater than the value of 100 kV/ms found in the literature for typical CDI systems (10, p. 95). The averages of the maximum and minimum measured voltages for the series of discharges were 139.5 kV and -143.812 kV respectively. The calculated duration of the likely main breakdown, arc and glow phases based on the recorded output of discharge 17 can be seen in figure 27. An average duration of 418.3 μs for the sum of these three phases of the 17 discharges and

a burning voltage of between 130 – 370 V for the arc and glow phases was also recorded.

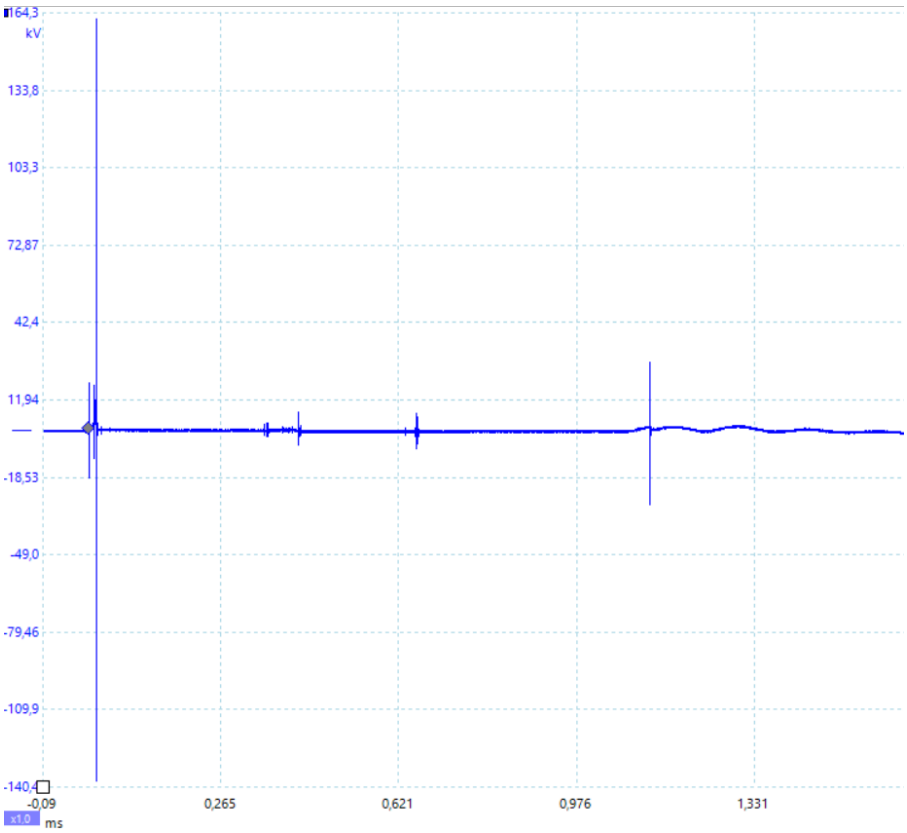

Figure 25. Typical voltage vs time plot of replicated circuit's ignition coil's high voltage output during CDI discharge.

Discharge type	CDI
Number of discharges in series	17
Average rise time (µs)	15.063
Average peak positive voltage (kV)	139.5
Average peak negative voltage (kV)	-143.8
Average rate of change during rise time (kV/µs)	9.3
Average breakdown, arc, and glow phase duration (µs)	418.282

Figure 26. Electrical characteristics of CDI-type discharge.

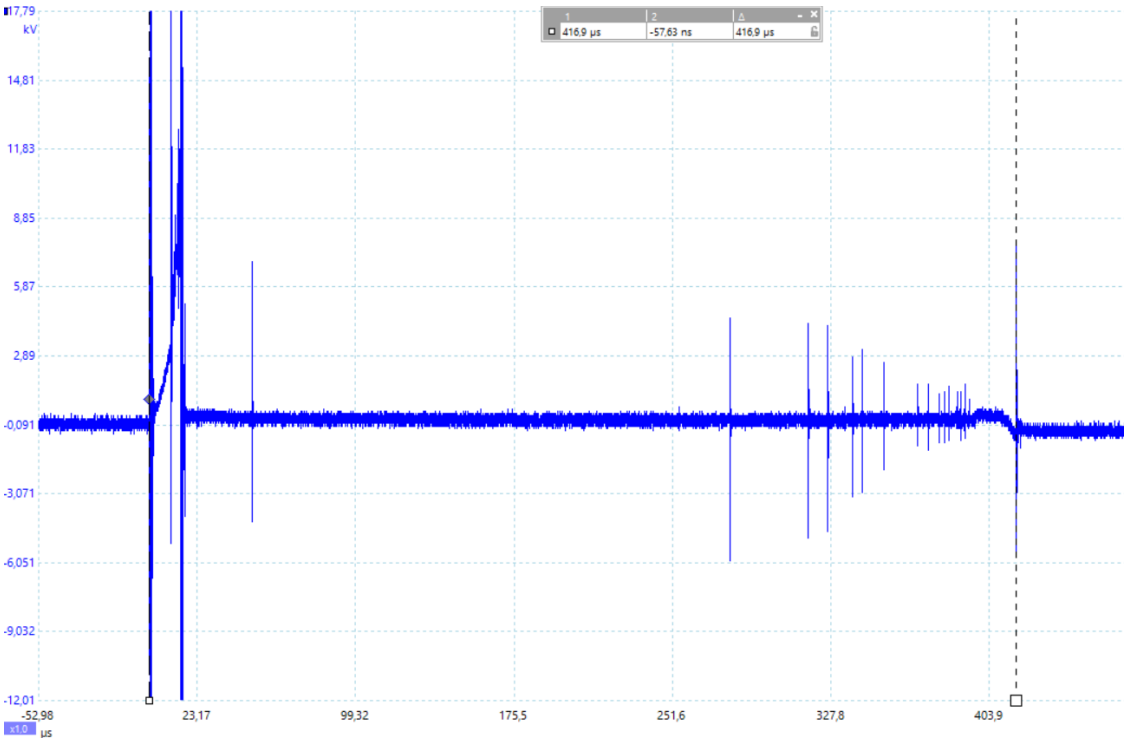

Figure 27. Calculated duration of the supposed breakdown, arc, and glow phases of CDI discharge 17.

The voltage trace produced by the CDI discharge also displayed unique characteristics. Following the apparent cessation of possible arc and glow phases, and stabilisation close to the zero-point, output voltage steadily increased before rising very quickly to high peak values, sometimes as much as approximately 27 kV, after which the output diminished finally in a damped oscillatory fashion. This can be seen in figure 28.

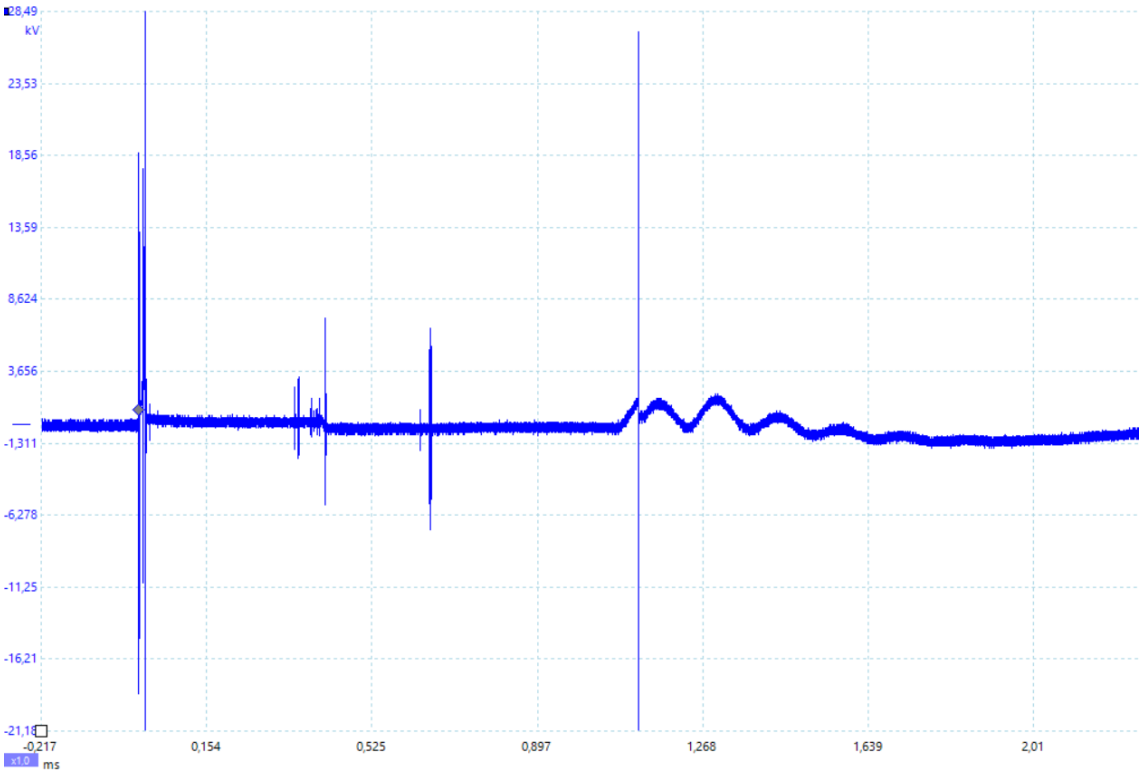

Figure 28. Secondary voltage peaks of replicated circuit's ignition coil's output voltage produced during CDI discharge.

3.3.2 Electrical Characteristics of Different Discharges: High Voltage Output of Ignition Coil with Plasma-Type Discharge

Figure 29 depicts a typical trace of voltage with respect to time produced by the output of the replicated circuit's ignition coil's secondary windings when the rectifier diode remains connected across the primary and secondary windings of the ignition coil, i.e., when the discharge at the spark gap is of the plasma-type. As can be seen in figure 30, the calculated average voltage rise time to the maximum measured positive value for the series of 6 discharges was 15.74 µs, which does not significantly differ from the value obtained from the series of CDI discharges.

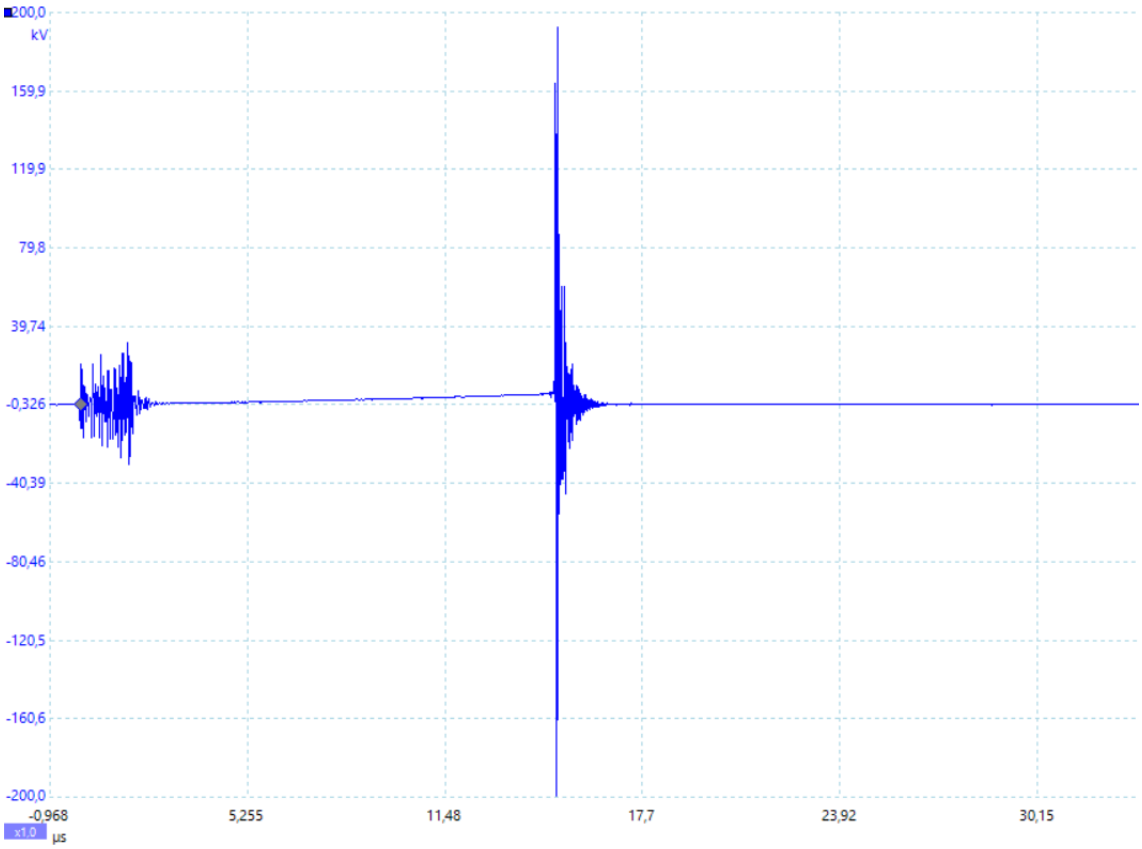

Figure 29. Typical voltage vs time plot of replicated circuit's ignition coil's high voltage output during plasma discharge.

Discharge type	Plasma
Number of discharges in series	6
Average rise time (µs)	15.74
Average peak positive voltage (kV)	191.36
Average peak positive voltage increase over CDI %	137.18
Average peak negative voltage (kV)	-200
Average peak negative voltage decrease over CDI %	139.07
Average rate of change during rise time (kV/µs)	12.16
Average discharge duration (µs)	17.596

Figure 30. Electrical characteristics of plasma discharge.

Several aspects of the results, however, differ significantly from the those obtained with a CDI discharge: the average rate of change during the rise time

was 12.16 kV/µs, while the average total time of the discharge event was calculated to be 17.59 µs, a fraction of the equivalent value obtained for only the assumed duration of the breakdown, arc and glow phases of the CDI discharge. The average of the maximum and minimum measured voltages for the entire series of discharges measured were 191,36 kV and -200 kV respectively, a 137.18 % and 139.07 % increase over the equivalent average values calculated for the CDI discharge series. Furthermore, as can be seen in figure 27, when the output voltage of the ignition coil's secondary windings settled back down to the zero point after an apparent breakdown, no further changes occurred in the output before the next discharge.

3.3.3 Characteristics of 47 µF 350 VDC Discharge Capacitor During CDI Discharge

Depicted in figure 28 is a typical trace of voltage with respect to time representing a CDI discharge event as measured from the terminals of the discharge capacitor. The average discharge time from the fully charged value of approximately 314.7 VDC to the lowest measured value for the series of 3 discharges was 363,13 µs. Typical electrical characteristics of the discharge capacitor during CDI-type discharge can be seen in figure 32. The figure displays the electrical characteristics of the discharge capacitor during the first of 3 discharges. The capacitor's calculated average discharge power over the 3 discharges, when discharging from the fully charged value to 150 VDC was -10.606 kW. The average time to discharge from 314.7 V to 150 V was 120.2 µs.

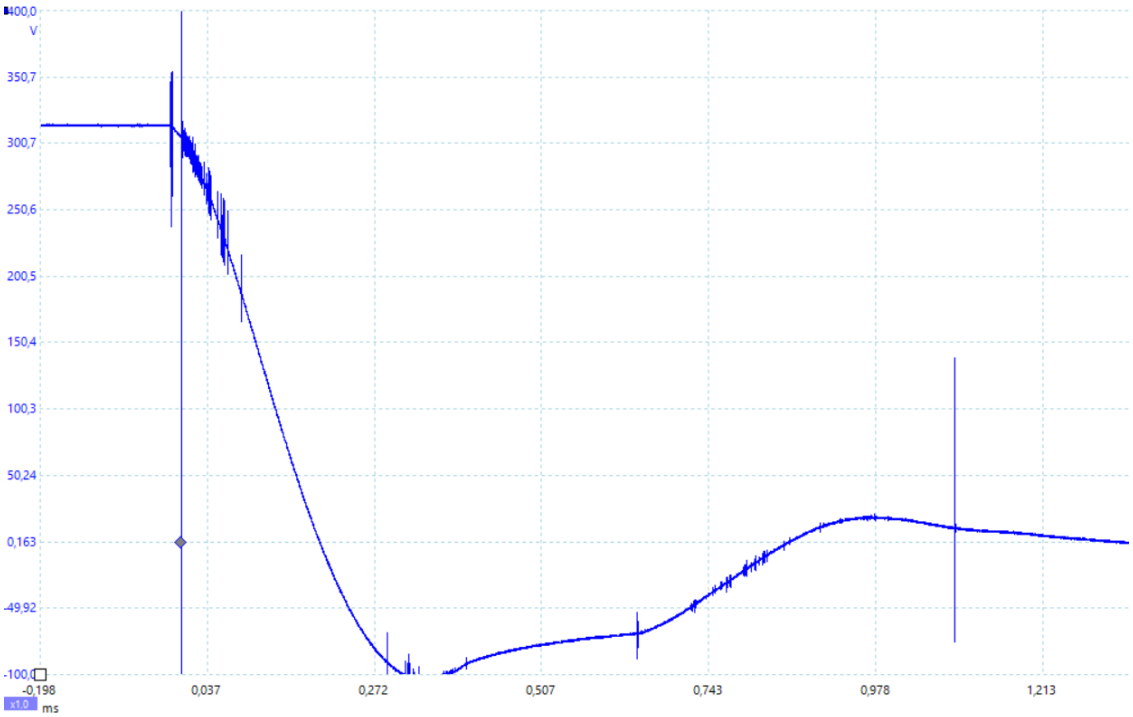

Figure 31. Typical voltage vs time plot of replicated circuit's discharge capacitor's output during CDI discharge.

Discharge capacitor properties CDI discharge 1	
Capacitance (F)	0.000047
Maximum capacitor voltage (VDC)	314,7
Discharge limit (VDC)	150
Difference (VDC)	-164.7
Time to discharge (s)	0.0001202
Voltage derivative over timestep $dv_c(t)/dt$ (VDC)	-1370216.31
Discharge current (A)	-64.40
Discharge power to limit (W)	-10606.71

Figure 32. Electrical characteristics of discharge capacitor during CDI discharge 1/3.

3.3.4 Characteristics of 47 µF 350 VDC Discharge Capacitor During Plasma Discharge

Depicted in figure 33, a typical trace of voltage with respect to time representing a plasma discharge event as measured from the terminals of the discharge capacitor can be seen. The average discharge time from the fully charged value of approximately 314.7 VDC to the lowest measured value for the series of 4

discharges was 354.825 µs, only slightly less than the value calculated for the series of CDI discharges. Typical electrical characteristics of the discharge capacitor during CDI discharge can be seen in figure 34. The figure displays the electrical characteristics of the discharge capacitor during the first of 4 discharges. The capacitor's calculated average discharge power over the 4 discharges, when discharging from the fully charged value to 150 VDC was -55.004 kW, 5.18 times greater in magnitude than the equivalent value calculated for CDI discharge. The average time to discharge from 314.7 V to 150 V was 23.2 µs, over 5.18 times less in magnitude than the equivalent value calculated for CDI discharge.

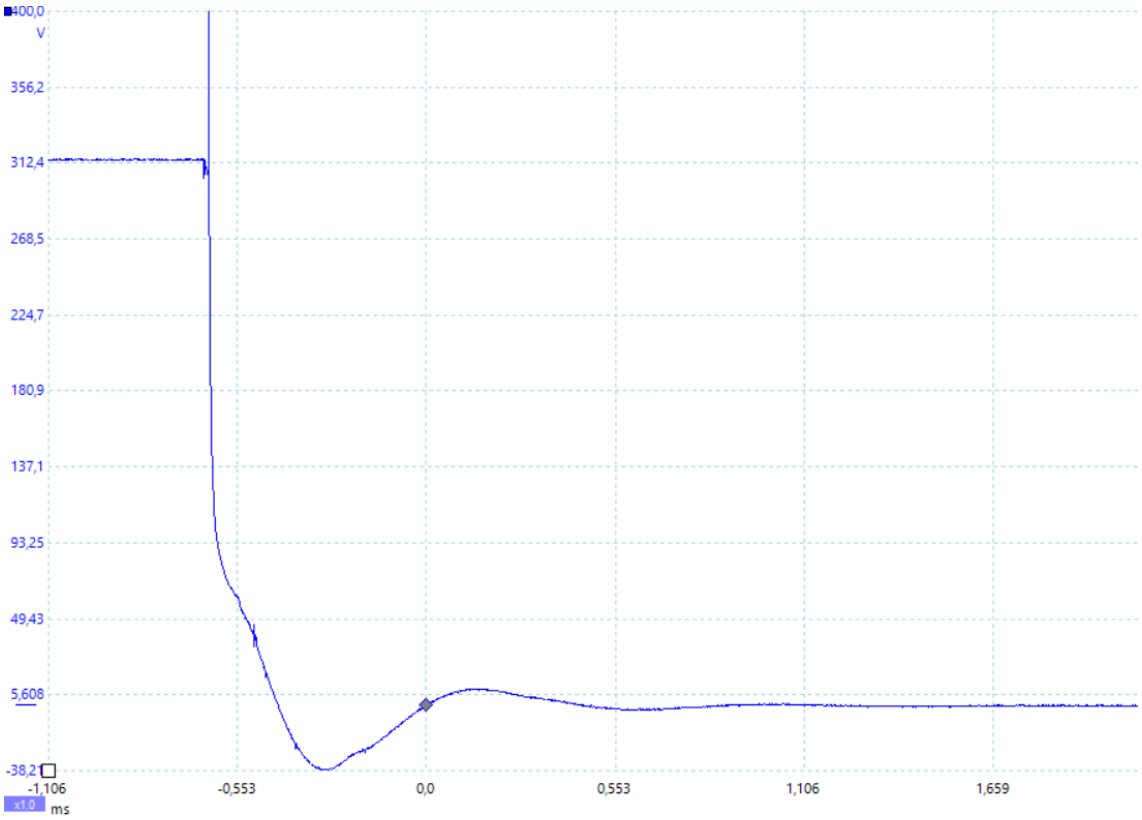

Figure 33. Typical voltage vs time plot of replicated circuit's discharge capacitor's output during plasma discharge.

Discharge capacitor properties plasma discharge 1	
Capacitance (F)	0.000047
Maximum capacitor voltage (VDC)	314.7
Discharge limit (VDC)	150
Difference (VDC)	-164.7
Time to discharge (s)	0.00002293
Voltage derivative over timestep dvc(t)/dt (VDC)	-7182730.05
Discharge current (A)	-337.59
Discharge power to limit (W)	-55600.80

Figure 34. Electrical characteristics of discharge capacitor during plasma discharge 1/4.

3.3.5 Comparison of Light Emission Produced by CDI, Plasma Discharges With 56 µF 400 V Discharge Capacitor

Pictured in figure 35, there is an example of visible light emission from a CDI discharge, where the 56 µF 400 V discharge capacitor has been charged to 357 VDC and most of the cathode has been removed, making the spark gap approximately 2.5 mm. Energy delivered to the primary windings of the ignition coil before losses was thus 3.57 J. Pictured in figure 36 is a comparative example of the visible light emission from a plasma discharge, where the same capacitor has been charged to a measured 354 VDC. Energy delivered before losses is therefore slightly less than in the case of the CDI discharge, at 3.5 J. The quantity and intensity of light emission from the plasma discharge appeared to be several orders of magnitude greater than that produced by the CDI discharge. As can also be seen figure 36, the light emission did not appear to be only contained to a region between the electrodes of the spark plug. Rather, it enveloped a significant region surrounding the electrodes and the fabricated ground contact extension, such than a large portion of the assembly appeared to be shrouded by the intensity of the emission.

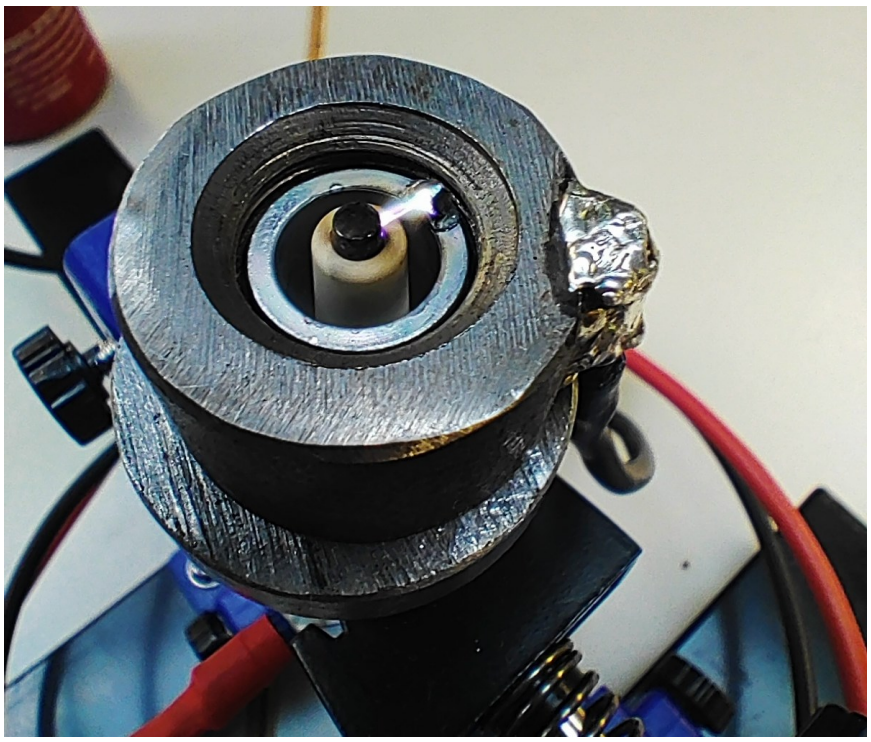

Figure 35. CDI discharge in air at 295.15 K, 56 μF discharge capacitor charged to 357 VDC, discharge energy before losses 3.57 J.

Figure 36. Plasma discharge in air at 295.15 K, 56 μF discharge capacitor charged to 354 VDC, discharge energy before losses 3.5 J.

3.3.6 Microscopic Electrode Surface Analysis: CDI Discharge

The electrodes of an NGK BP5ES spark plug are depicted in figure 37 and figure 38. In this case, the spark plug was fired for 1 hour at 2.024 Hz with the discharge capacitor charged to a voltage of 357 VDC, where the discharge type was CDI and the gap between the electrodes was 1 mm. Damage to both the cathode and the anode was evident: both the cathode and the anode exhibited evidence of excessive heating, however, particularly the cathode displayed traits associated with hot spots. Heavy discolouration close to the periphery of the anode and possible pitting and/or crater formation are indications of repeated recombination of highly energised of electrons occurring in this area, whereas lighter discolouration and removal of oxide layer only suggests less frequent discharge activity.

The region of the cathode photographed in figure 38 shows signs of heavy erosion. Evidence of cooling and solidification of molten nickel-alloy electrode material after liquification can be seen. Dispersion of material around the edges of the region subjected to a high concentration of discharges is also apparent in figure 38.

The electrodes of another NGK BP5ES spark plug can be seen in figure 39 and 40. In this case, the gap spacing of 1 mm used for the previous discharge analysis remained the same, whereas the discharge capacitor was charged to 199.5 VDC and the spark plug was fired once. Energy delivered before losses was, therefore, 1.11 J. Clear evidence of damage to either of the electrodes after the discharge is indiscernible from the figures.

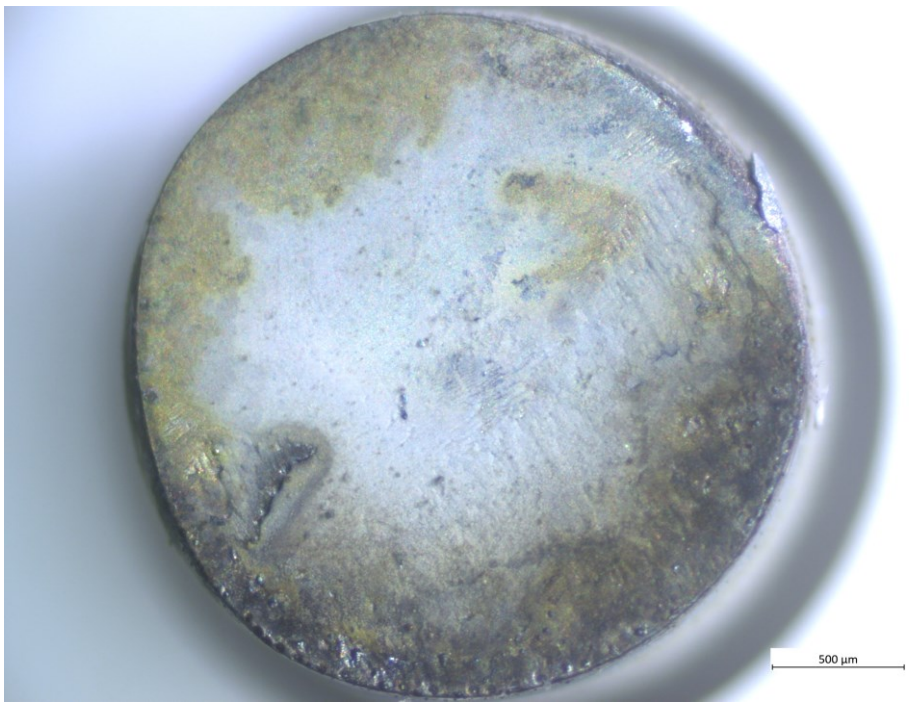

Figure 37. Anode of NGK BP5ES spark plug after firing CDI-type discharges for 1 hour at 2.024 Hz with the discharge capacitor charged to 357 VDC. Discharge energy before losses was 3.57 J. Distance between electrodes was 1 mm.

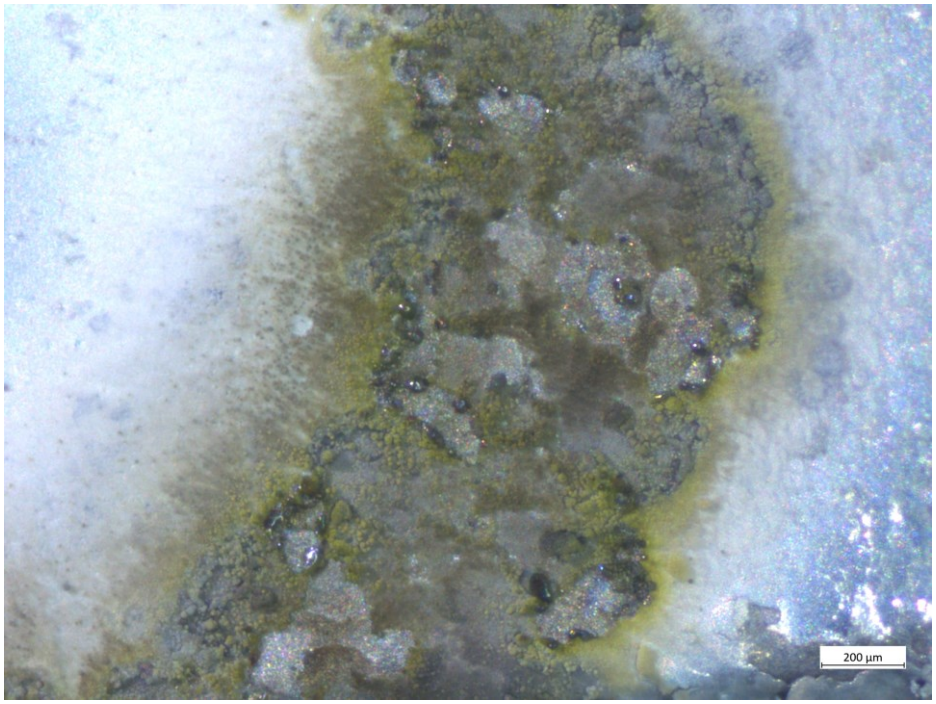

Figure 38. Cathode of NGK BP5ES spark plug after firing CDI-type discharges for 1 hour at 2.024 Hz with the discharge capacitor charged to 357 VDC. Discharge energy before losses was 3.57 J. Distance between electrodes was 1 mm.

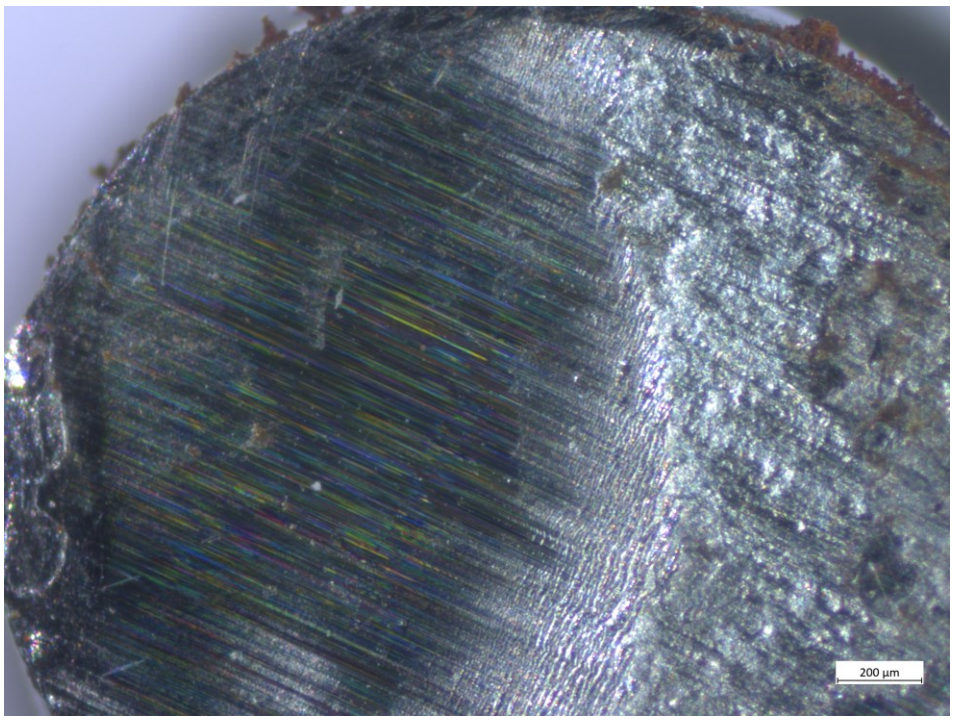

Figure 39. View of NGK BP5ES spark plug's anode after firing of single CDI-type discharge with the discharge capacitor charged to 199.5 VDC. Discharge energy before losses was 1.11 J. Distance between electrodes was 1 mm.

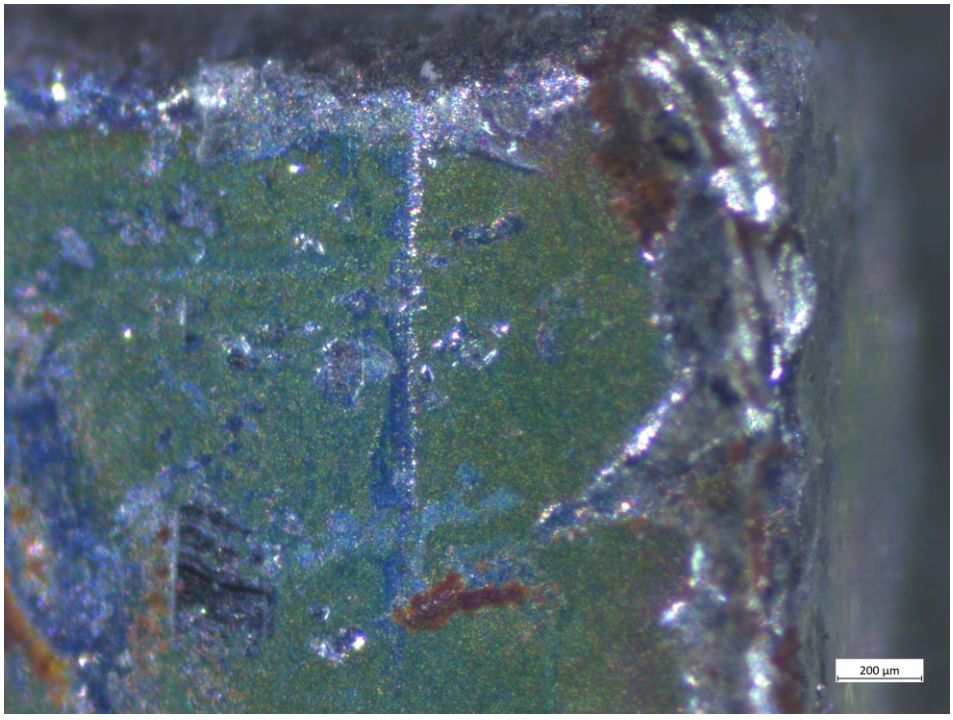

Figure 40. View of NGK BP5ES spark plug's cathode after firing of single CDI-type discharge, with the discharge capacitor charged to 199.5 VDC. Discharge energy before losses was 1.11 J. Distance between electrodes was 1 mm.

3.3.7 Microscopic Electrode Surface Analysis: Plasma Discharge

The electrodes of an NGK BP5ES spark plug are depicted in figure 41 and figure 42. In this case, the spark plug was fired for 1 hour at 2.024 Hz with the discharge capacitor charged to a voltage of 354 VDC, where the discharge type was plasma and the gap between the electrodes measured 1 mm. Evidence of extreme damage to both the anode and cathode can be seen in the figures. Both electrodes exhibited evidence of excessive heating, however, once again, particularly the cathode displayed traits of more extreme wear and erosion. As can be seen in figure 42, most of the surface was covered with significant undulations and roughness. The image suggests large regions of the cathode underwent liquefication and possibly vaporisation followed by rapid cooling and solidification of the nickel-alloy cathode material during the discharges. Additionally, compared to the electrodes used to produce the equivalent CDI-type discharges, no part of the electrodes remained undamaged and both cathode and anode displayed evidence of intense burning of the nickel-alloy electrode material's oxide layer.

In contrast to the equivalent CDI-type discharge produced, figures 43 and 44 depict clear evidence of damage to both electrodes after one discharge of the plasma type, where the discharge capacitor had been charged to 200.2 V and the gap between the electrodes was kept at 1 mm. A relatively large area on the surface of the cathode and the anode appears to have been heated intensely and the material in this area has possibly undergone a phase change during the heating event. In the case of the cathode, this area measures over 500 μm in diameter. Microscopic imaging of the electrodes of yet another NGK BP5ES spark plug after firing three plasma-type discharges, where the discharge capacitor had been charged to a similar 200 V, but the gap between the electrodes had been increased to 2 mm, can be seen in figures 43 and 44 in appendix 1. The cathode and the anode both sustained damage consistent with the electrodes used to fire the single plasma-type discharge over a 1 mm gap.

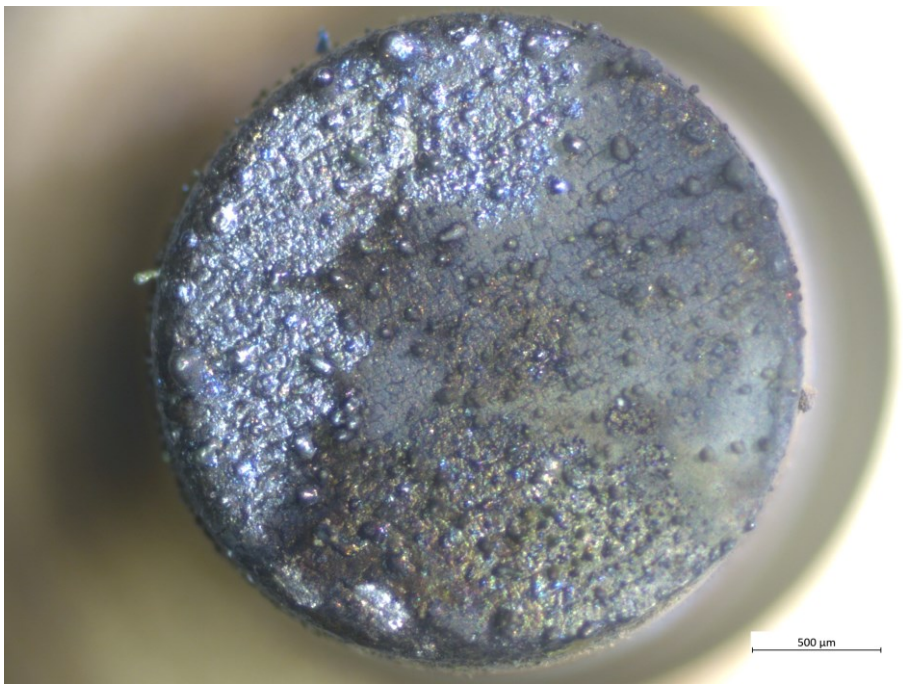

Figure 41. Anode of NGK BP5ES spark plug after firing plasma-type discharges for 1 hour at 2.024 Hz with the discharge capacitor charged to 354 VDC. Discharge energy before losses was 3.5 J. Distance between electrodes was 1 mm.

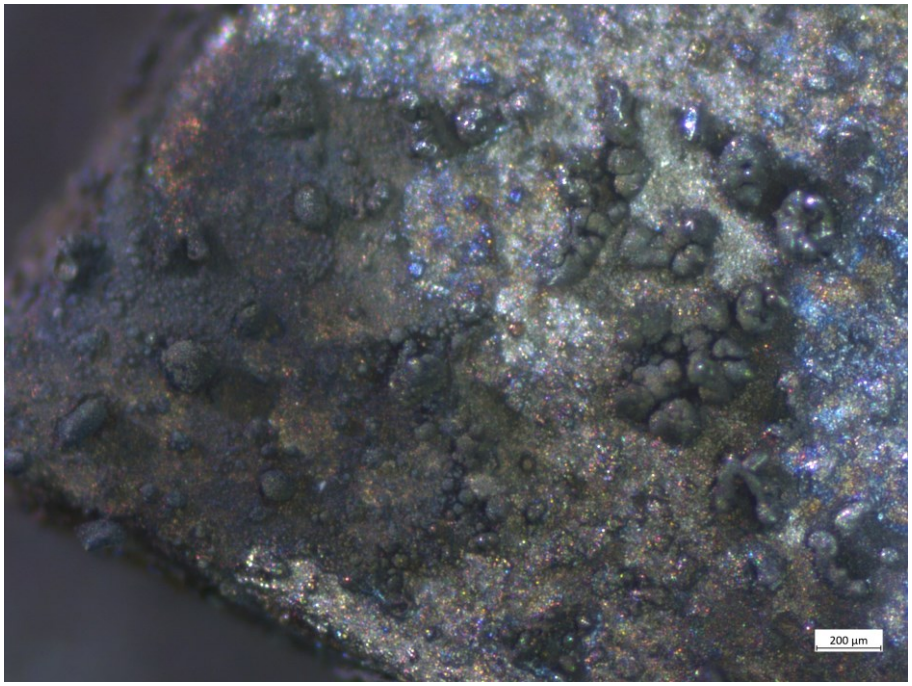

Figure 42. Cathode of NGK BP5ES spark plug after firing plasma-type discharges for 1 hour at 2.024 Hz with the discharge capacitor charged to 354 VDC. Discharge energy before losses was 3.5 J. Distance between electrodes was 1 mm.

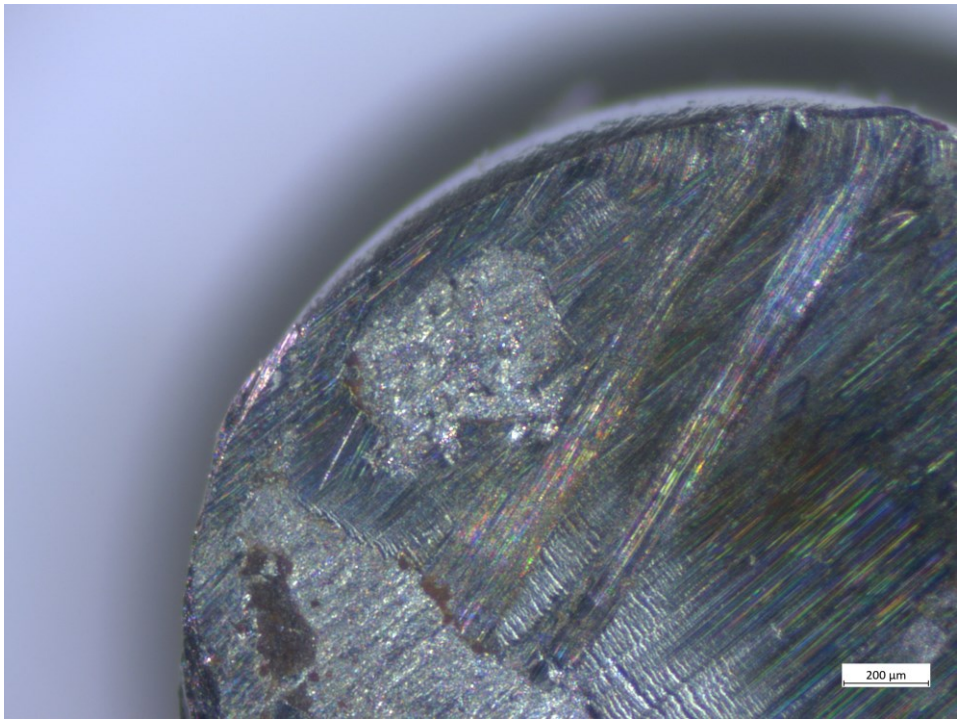

Figure 43. View of NGK BP5ES spark plug's anode after firing of single plasma-type discharge with the discharge capacitor charged to 200.2 VDC. Discharge energy before losses was 1.122 J. Distance between electrodes was 1 mm.

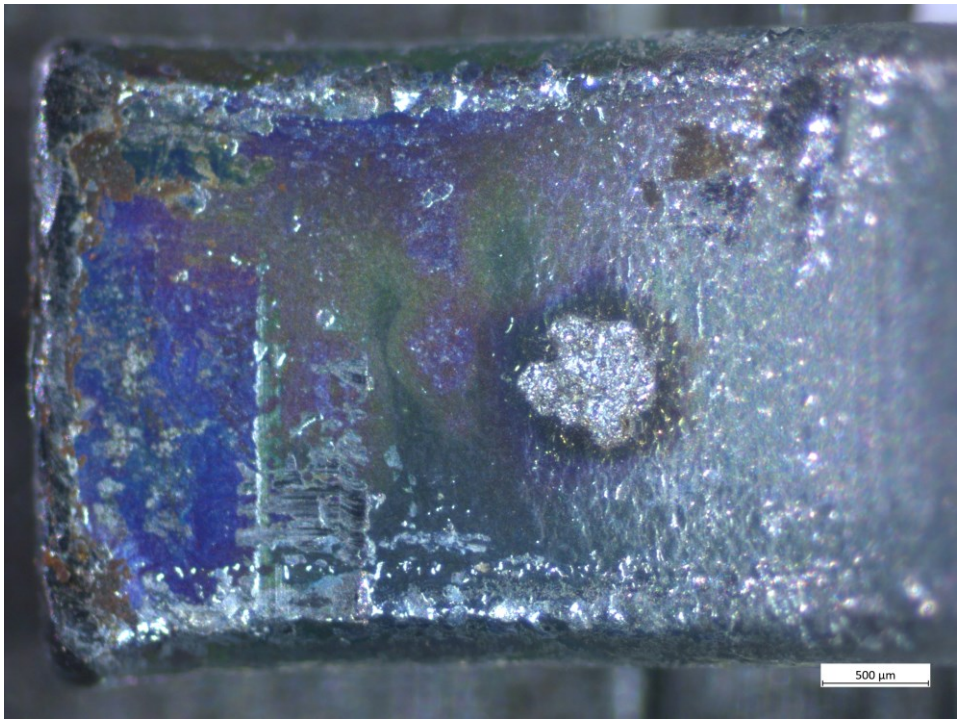

Figure 44. View of NGK BP5ES spark plug's anode after firing of single CDI discharge with the discharge capacitor charged to 200.2 VDC. Discharge energy before losses was 1.122 J. Distance between electrodes was 1 mm.

3.4 Discussion

Due to the lack of EMI suppressing cables used in the replicated circuit, the results presented in chapters 3.3.1 and 3.3.2 must be taken critically. Without comparing the results to those taken with a different oscilloscope and probe, with some measures taken to suppress the ignition circuit's EMI output during discharge, in particular the values recorded for peak positive and negative output voltages, and in the case of CDI-type discharge, subsequent secondary peak positive and negative voltages, must be scrutinised. During some of the discharges, both positive and negative peaks exceeded the limits of the measurement range (+ 200 kV, - 200 kV), which is far more than the majority of values found in the literature, where typical maximum values for the output of a CDI system's ignition coil's secondary windings are below 100 kV (5, p. 1926). Such a high voltage may result in the lifespan of the ignition coil being severely shortened, however, sufficient data were not collected to verify or invalidate this point. The average duration of assumed breakdown, arc and/or glow phases recorded, however, is not inconsistent with values found in the literature, where Maly (10, p. 93) reports a duration of approximately 350 µs for a complete CDI discharge in air at a pressure of 2 bar and at a temperature of 300 K. Reported burning voltages of ≅ 50 V for the arc phase and ≅ 500 V for the glow phases, however, are considerably less than those recorded in this investigation (130 – 370 V) (10, p. 101, p. 104).

The short duration of the complete plasma-type discharge and the partial discharge of the discharge capacitor during plasma-type discharge can be at least partially accounted for based on the patented circuit's unique design. The nature of the design is such, that, when the rectifier diode is connected, a lower resistance path to ground exists than through the ignition coil, meaning that if the gap has been sufficiently ionised, a portion of the energy stored within the discharge capacitor can more efficiently discharge across the gap, potentially decreasing overall discharge time compared to other ignition circuits.

The short discharge duration is a critical factor in bringing about the circuit's high power output and likely the plasma-type discharge's unique characteristics. Power can be expressed as

$$P = \frac{dW}{dt}. \quad (5)$$

W is work.
t is time.

This short discharge duration can be attributed to the circuit's overall low impedance and possibly extremely low resistance spark plug gap after breakdown. Firstly, the upper limit of the discharge current is only determined by the external impedances of the circuit (in this case, gap, spark plug, cables, connectors etc.) (9, p. 14; 10, p. 101). The overall impedance of the replicated ignition circuit was particularly low, as resistorless spark plugs were used, in addition to pure copper cabling without any EMI suppressing resistors or equivalent resistive material. Moreover, during the breakdown phase, Achat and colleagues (76, p. 666) note that if the voltage is sufficiently high a negative resistance situation emerges favourable to the development of an arc. It can be inferred that conditions in the gap of the replicated circuit are particularly favourable to the formation of an arc, thus giving rise to a high current, low voltage component of the discharge. This was indeed evident in the high discharge currents calculated from the measurements taken of the discharge capacitor's voltage during plasma-type discharge.

There are many similarities between the characteristics of the circuit examined in this study, in terms of its electrical properties and circuit design, and the characteristics of circuits used in the literature for plasma jet ignition systems. In both cases, a capacitor is used to discharge a low voltage, high current across the gap once the dielectric strength of the gas occupying the gap has been overcome by a high voltage, low current pulse from a high voltage transformer (50, p. 3). The plasma jet ignitor produces a hot jet-like flame kernel during the combustion process that extends from the ground electrode of the ignitor further than a conventional flame (52, p. 841), and, given the visual evidence of the

behaviour of the plasma-type discharge produced by the ignition circuit investigated in the results presented, it can be assumed that this kind of discharge may have a similar influence on flame kernel propagation during combustion in a pressurised combustion chamber. Furthermore, the electrodes of the spark plugs used to fire plasma-type discharges exhibited extreme erosion characteristics reminiscent of those reported in the literature for plasma-jet ignitors. One study found the measured erosion rates limited ignitor lifetimes to less than 10 hours (thus prohibitively high for conventional IC engine operation); it was not possible in the course of this study to conduct quantitative measurements of the used spark plug's erosion rates and on this basis estimate spark plug lifetimes, however, clearly visual inspections suggest a limitation to the operational duration of an ignitor when the investigated ignition circuit is in use (53, p. 792).

Evidence of intense heating of particularly the cathode and the cathode material undergoing phase changes, where the material has liquefied and possibly reached its boiling point, strongly suggests the presence of a powerful arc phase during the discharge, during which repeated high temperature electron emission via thermionic, field, or thermo-field emission and joule heating has occurred (27, p .140). The significance of other phases and how they contribute to the character of the discharge is difficult to determine without more sophisticated and nuanced measurements, measurement apparatuses and techniques. Based on the data obtained and the strong indication of the presence of an arc phase, in addition to knowledge of the characteristics of the arc phase, however, it can be assumed that a significant portion of the plasma created by the discharge is equilibrium in nature i.e., high temperature plasma, which consists of electrons, neutrals and ions in thermodynamic equilibrium.

The advantages and disadvantages of utilising PAI/PAC with low-temperature, non-equilibrium plasma and high-temperature, equilibrium plasma were presented in the literature reviewed. The disadvantages of utilising PAI/PAC with equilibrium plasma appeared to outweigh the benefits, according to several authors (54, p. 25; 45, p. 1526 – 1528; 53, p. 790; 63, p. 170). No literature focusing on the evaluation of the performance and characteristics of specifically the circuit examined in the present work was found, and as such, no substantial

conclusions based on the present work can be drawn with respect to its suitability in an automotive or otherwise real-world application and any possible advantages and/or disadvantages gained by utilising it before more extensive testing has been carried out.

3.5 Conclusion

In this thesis, published literature on different automotive ignition systems and their characteristics and performance; ignition spark formation theory and research; plasma properties; plasma theory and research in the context of ignition systems and ignition and combustion enhancement for internal combustion engines; as well as plasma properties of enhanced ignition systems for automotive applications were reviewed. A patented circuit designed to enhance the ignition/combustion process by utilising high energy plasma was replicated and its performance was measured and evaluated. The results, findings and theories in the reviewed material pertaining to plasma-jet ignition systems and the characteristics of CDI ignition systems, the arc discharge and the properties and behaviour of thermal, equilibrium plasma agreed to some extent with the experimental findings of the present study, however, further investigation is required for more comprehensive verification of these findings. Future studies should include testing of the replicated circuit on an automotive internal combustion engine and measuring the engine's power and torque outputs in addition to emissions. Moreover, measurements of the circuit's discharge current during a plasma-type discharge should be performed, as well as measurements of both the rates of active radical formation and the quantity produced during discharge events. Calorimetry should also be carried out to determine the electrical-to-thermal energy conversion efficiency for single discharges, whilst more insights could be gained into the erosion rates of ignitors used to produce the circuit's plasma-type discharges by determining the wear rate of the ignitor's electrodes in terms of coulombs of charge per gram of material eroded.

References

1 Rief, Konrad. 2015. Gasoline Engine Management: Systems and Components. Ebook: Springer Viewg.

2 Juhala, Matti; Lehtinen, Arto; Suominen, Matti; Tammi, Kari. 2005. Moottorinalan sähköoppi. Jyväskylä: Gummerus Kirjapaino Oy.

3 Hong, Alice & Elert, Glenn. 2000. The Physics Factbook: Dielectric Strength of Air. Online material. <https://hypertextbook.com/facts/2000/AliceHong.shtml>. Viewed 3.3.2022.

4 Reif, Konrad & Dietsche, Karl-Heinz et. al. 2014. Automotive Handbook. Stuttgart: Robert Bosch GmbH.

5 Mon, Su Su Yi. 2019. Capacitive Discharge Ignition (CDI) System for Spark Ignition (SI) Engine (Pulse Control Circuit). International Journal of Trend in Scientific Research and Development (IJTSRD). Vol. 3, issue 5, s. 1925-1929.

6 Shano, Charles L; Hufton, Arthur G. 1967. Capacitor Discharge Ignition – A Design Approach. Automotive Engineering Congress Detroit, Michigan. January 9-13, 1967. SAE International.

7 Šimakauskas, Audris. 2014. Research of the SI Engine With Multispark Capacitor Discharge Ignition System. Agricultural Engineering, Research Papers. Vol. 26, No. 1, p. 104-115.

8 Williamson, Terrence L. 1971. Ignition System Requirements and Their Application to the Design of Capacitor Discharge Ignition Systems. Bachelor's thesis. National Technical Information Service.

9 Jeanvoine, Nicholas. 2009. Plasma-material interaction and Electrode Degradation in High Voltage Ignition Discharges. Dissertation. University of Saarland.

10 Maly, Rudolf. 1984. Spark Ignition: Its Physics and Effect on the Internal Combustion Engine. Fuel Economy, p. 91-48.

11 Huang, S; Li, T; Ma, P; Xie, S; Zhang, Z. & Chen, R. 2019. Quantitative Evaluation of the Breakdown Process of Spark Discharge for Spark-Ignition Engines. Journal of Physics D: Applied Physics.

12 Lee, M. J; Hall, M; Ezekoye, O. A. & Matthews, R. D. 2005. Voltage, and Energy Deposition Characteristics of Spark Ignition Systems. SAE Technical Paper Series.

13 Townsend Discharge. Online material. Wikipedia. <https://en.wikipedia.org/wiki/Townsend_discharge>. Updated 23.12.2021. Viewed 24.3.2022.

14 Chung, Kyoung-Jae. 2018. Electrical Breakdown in Gases. Online lecture material. Department of Nuclear Engineering, Seoul National University. < https://ocw.snu.ac.kr/sites/default/files/NOTE/Lecture_06_Electrical%20breakdown%20in%20gases.pdf>. Viewed 1.4.2022.

15 Paschen Curve: Voltage Breakdown vs Pressure. Online material. High Voltage Connection. < http://highvoltageconnection.com/articles/paschen-curve.html>. Viewed 31.3.2022.

16 Paschen's law. Online material. Wikipedia. <https://en.wikipedia.org/wiki/Paschen%27s_law>. Updated 31.3.2022. Viewed 31.3.2022.

17 Bowker, H. C. 1931. Variation of spark-potential with temperature in gases. Proceedings of the Physical Society, 43(1), p. 96-112.

18 Bohzenkov, S. A., Starikovskaia, S. M., & Starikovskii, A. Y. 2003. Nanosecond gas discharge ignition of H2- and CH4- containing mixtures. Combustion and Flame, 133(1-2), p. 133-146.

19 Meek, J. M.; Craggs, J. D. 1953. Electrical Breakdown of Gases. Oxford: Clarendon Press.

20 Loeb, L. B. 1960. Basic Processes of Gaseous Electronics. Berkely: University of California Press.

21 Raether, H. 1964. Electron Avalanches and Breakdown in Gases. London: Butterworths.

22 Sigmond, R. S. 1984. The residual streamer channel: Return strokes and secondary streamers. Journal of Applied Physics, 56(5), 1355-1370.

23 Marode, E. 1975. The mechanism of spark breakdown in air at atmospheric pressure between as positive point and a plane. I. Experimental: Nature of streamer track. Journal of Applied Physics, 46(5), 2005-2015.

24 Starikovskaia, S. M. 2006. Plasma assisted ignition and combustion. Journal of Physics D: Applied Physics, 39(16), p. 265-299.

25 Ono, R., & Oda, T. 2003. Formation and structure of primary and secondary streamers in positive pulsed corona discharge- effect of oxygen concentration and applied voltage. Journal of Physics D: Applied Physics, 26(16), p. 1952-1958.

26 Maly, R; Vogel, M. 1979. Initiation and propagation of flame fronts in lean CH4-air mixtures by the three modes of the ignition spark. Symposium (International) on Combustion, 17(1), p. 821-831.

27 Heiberlein, J. V. R; Kimblin, C. W.& Lee, A (Ed. Browne, T. E.). 1984. Nature of the Electric Arc, in Circuit Interruption, Theory and Technique.New York: Marcel Dekker.

28 Kim, K., & Askari, O. 2019. Understanding the Effect of Capacitive Discharge Ignition on Plasma Formation and Flame Propagation of Air-Propane Mixture. Journal of Energy Resources Technology., 141(8), 082201.

29 Slade, P. G (Ed. Slade, P. G.). 1999. The Arc and Interruption, in Electrical Contacts: Principles and Applications. New York: Marcel Decker.

30 Wasa, K., Hayakawa, S. 1992. Handbook of Sputter Deposition Technology: Principles, Technology and Applications (Materials Science and Process Technology Series). United States: William Andrew Inc.

31 Corrigan, D. J; Pascolini, E; Zecchetti, D. & Titus, F. 2017. Ignition system development for High-Speed High Load Lean Boosted Engines. Ignition Systems for Gasoline Engines: 3rd International Conference, November 3-4, 2016, Berlin, Germany.

32 Teets, R. E., & Sell, J. A. 1988. Calorimetry of Ignition Sparks. SAE Transactions vol. 97, Section 6: Journal of Engines. p. 371-383.

33 Rohwien, J. G; Babcock, S. R; Butram, M. T. 1995. Advanced automotive ignition systems. Digest of Technical Papers. Tenth IEEE International Pulsed Power Conference.

34 Holden, H. 2013. Capacitive Discharge Ignition vs Magnetic Discharge Ignition: Ignition System Options for the TR4A. Online material. < http://nebula.wsimg.com/a0048958fdda77c4862ad82c764ec88b?AccessKeyId=967E22DE049163134A29&disposition=0&alloworigin=1>. Viewed 4.4.2022. Updated 2015.

35 Kim, K; Hall, M. J; Wilson, P. S. 2020. Arc Phase Spark Plug Energy Deposition Characteristics Measured Using a Spark Plug Calorimeter Based on Differential Pressure Measurement. Energies, 13 (14), 3550.

36 Goebel, D. M; Katz, I. 2008. Fundamentals of Electric Propulsion: Ion and Hall Thrusters. Ebook: John Wiley & Sons.

37 Inan, U. S; Golkowski, M. 2011. Principles of Plasma Physics for Engineers and Scientists. Cambridge: Cambridge University Press.

38 Karttunen, S. 1991. Plasmafysiikan perusteet. Raportti TKK-F-B134 28.6.1991. Valtion teknillinen tutkimuskeskus.

39 Gibbon, P. (Ed. B. Holzer). 2014. Introduction to Plasma Physics. Proceedings of the CAS-CERN Accelerator School: Plasma Wake Acceleration, Geneva, Switzerland, 23-29 November 2014. CERN-2016-001.

40 Fitzpatrick, R. 2016. Plasma Physics. Online material. The University of Texas. <https://farside.ph.utexas.edu/teaching/plasma/Plasma/index.html>. Viewed 5.4.2022.

41 Binding energy. Online material. Wikipedia. <https://en.wikipedia.org/wiki/Binding_energy>. Updated 9.8.2022. Viewed 25.4.2022.

42 Boulos, M. I; Fauchais, P. & Pfender, E. 1994. Thermal Plasmas: Fundamentals and Applications: Volume 1. New York and London: Plenum Press.

43 Starikovskaia, S. M. 2014. Plasma-assisted ignition and combustion: nanosecond discharges and development of kinetic mechanisms. Journal of Physics D: Applied Physics, 47(35), 353001.

44 Tardiveau, P; Marode, E; Agneray, A. & Cheaib, M. 2001. Pressure effects on the development of an electric discharge in non-uniform fields. Journal of Physics D: Applied Physics. 34(11), 1690-1696.

45 Asik, J. R; Piatkowski, P; Foucher, M. J. & Rado, W. G. 1977. Design of a Plasma Jet Ignition System for Automotive Application. SAE International, 770355, p. 1516-1530.

46 Weinberg, F. J. 1978. Ignition by Plasma Jet. Nature, Vol. 272. 23 March 1978. p. 341-343.

47 Yoshida, K; Shoji, H & Takana. H. 1999. Performance of newly developed Plasma Jet Igniter. Proceedings of the 1999 SAE Small Engine Technology Conference. SAE 1999-01-3327.

48 Gao, H; Matthews, R. D; Hall, M. J. & Hari, S. From Spark Plugs to Railplugs – The Characteristics of a New Ignition System. SAE Technical Paper Series. Reprinted From: SI Engine Experiment and Modelling (SP-1901).

49 Giannini, G. M. 1957. The Plasma Jet. Scientific American Vol. 197, No. 2. p. 80-90.

50 Dale, J. D; Oppenheim, A. K. 1981. Enhanced Ignition for I.C. Engines With Premixed Gases. SAE Technical Paper Series.

51 Orrin, J. E; Vince, I. M. & Weinberg, F. J. 1981. A Study of plasma jet ignition mechanisms. Symposium (International) on Combustion, 18(1), p. 1757-1765.

52 Choe, M. S; Lee, K. T; Kim, K. S. & Choi, D. S. 2020. Effect of the Plasma Jet Ignition and Flame Kernel Under the Combustion Process in a Constant Volume Combustion Chamber. International Journal of Automotive Technology, Vol. 21, No. 4. p. 833–842.

53 Smy, P. R; Clements, R. M; Dale, J. D; Simeoni, D. & Topham, D. R. 1983. Efficiency and erosion characteristics of plasma jet igniters. Journal of Physics D: Applied Physics, 16(5), p. 783–791.

54 Ju, Y., & Sun, W. 2015. Plasma assisted combustion: Dynamics and chemistry. Progress in Energy and Combustion Science, 48, p. 21–83.

55 Ziegler, G. F. W; Wagner, E. P; Saggau, B. & Maly, R. 1984. Influence of a Breakdown Ignition System on Performance and Emissions Characteristics. SAE Technical Papers Series.

56 Anderson, R. W. 1987. The Effect of Ignition system Power on Fast Burn Engine Combustion. SAE technical paper series.

57 Modien, R. M; Checkel, M. D. & Dale, J. D. 1991. The Effect of Enhanced Ignition Systems on Early Flame Development in Quiescent and Turbulent Conditions. SAE Technical Paper Series. International Congress and Exposition, Detroit, Michigan February 25-March 1, 1991. 910564.

58 Air-fuel ratio. Wikipedia. Online material <https://en.wikipedia.org/wiki/Air%E2%80%93fuel_ratio>. Updated 30.9.2022. Viewed 28.4.2022.

59 Shiraishi, T; Urushihara, T & Gundersen, M. 2009. A trial of ignition innovation of gasoline engine by nanosecond pulsed low temperature plasma ignition. Journal of Physics D: Applied Physics, 42(2009), 135208 (12 pp).

60 Sevik, J; Wallner, T; Pamminger, M; Scarcelli, R; Singleton, D. & Sanders, J. 2016. Extending Lean and Exhaust Gas Recirculation-Dilute Operating Limits of a Modern Direct-Injection Engine Using a Low-Energy Transient Plasma Ignition System. Journal of Engineering for Gas Turbines and Power, 138(11), 112807.

61 Sjöberg, M; Zeng W; Singleton, D; Sanders, J. M, & Gundersen, M. A. 2014. Combined Effects of Multi-Pulse Transient Plasma Ignition and Intake Heating on Lean Limits of Well-Mixed E85 DISI Engine Operation. SAE International Journal of Engines, 7(4), 1781–1801.

62 Singleton, D; Pendleton, S. J & Gundersen, M. A. 2010. The role of non-thermal transient plasma for enhanced flame ignition in C2H4-air. Journal of Physics D: Applied Physics, 44(2), 022001.

63 Ikoto, I; Wolk, B. 2017. Calorimetry and Atomic Oxygen Laser-Induced Fluorescence of Pulsed Nanosecond Discharges at Above-Atmospheric Pressures. Ignition Systems for Gasoline Engines: 3rd International Conference, November 3-4, 2016, Berlin, Germany. p

64 Arrhennius equation. Online material. Wikipedia. <https://en.wikipedia.org/wiki/Arrhenius_equation>. Updated 7.8.2022. Viewed 7.7.2022.

65 Dale, J. 1997. Application of high energy ignition systems to engines. Progress in Energy and Combustion Science, 23(5-6), 379–398.

66 Harrington, J. A; Shishu, R. C. & Asik, J. R. 1974. A Study of Ignition System Effects on Power, Emissions, Lean Misfire Limit, and EGR Tolerance of a Single Cylinder Engine – Multiple Spark versus Conventional Single Spark Ignition. SAE Technical Paper Series.

67 Starikovskii, A. Y; Anikin, N. B; Kosarev, I. N; Mintoussov, E. I; Nudnova, M. M; Rakitin, A. E; Roupassov, D. V; Starikovskaia, S.M; & Zhukov, V. P. 2008. Nanosecond-Pulsed Discharges for Plasma-Assisted Combustion and Aerodynamics. Journal of Propulsion and Power, 24(6), 1182–1197.

68 Adamovich, I. V; Choi, I; Jiang, N; Kim, J.-H.; Keshav, S; Lempert, W. R; Mitsunov, E; Nishihara, M; Samimy, M; & Uddi, M. 2009. Plasma assisted ignition and high-speed flow control: non-thermal and thermal effects. Plasma Sources Science and Technology, 18(3), 034018.

69 Kosarev, I. N; Aleksandrov, N. L; Kindysheva, S. V; Starikovskaia, S. M. & Starikovskii, A. Y. (2008). Kinetic mechanism of plasma-assisted ignition of hydrocarbons. Journal of Physics D: Applied Physics, 41(3), 032002.

70 Uddi, M; Jiang, N; Mitsunov, E; Adamovich, I. V. & Lempert, W. R. 2009. Atomic oxygen measurements in air and air/fuel nanosecond pulse discharges by two photon laser induced fluorescence. Proceedings of the Combustion Institute, 32(1), 929–936.

71 Cathey, C. D; Tang, T; Shiraishi, T; Urushihara, T; Kuthi, A. & Gundersen A. Nanosecond Plasma Ignition for Improved Performance of an Internal Combustion Engine. IEEE Transactions on Plasma Science, 35(6), 1664-1668.

72 Sacarelli, R; Zhang, A; Wallner, T; Breden, D; Karpatne, A; Raja, L & Wolk, B. 2018. Multi-dimensional Modelling of Non-equilibrium Plasma for Automotive Applications. SAE Technical Paper Series.

73 Sirinivasan, A; Ramanathan, K; Choquette, L; Murakami, A. 2013. US8555867B2: Energy efficient plasma generation. Patent. < https://patents.google.com/patent/US8555867>. Viewed 25.3.2022.

74 Plasma Ignition – Water Sparkplug Circuit by Peter Lindemann. Online material. YouTube. <https://www.youtube.com/watch?v=vOhNtRhJ5Rw>. Viewed 30.3.2022.

75 Bi-Power Relays LY Datasheet. Online material. Omron. < https://www.ia.omron.com/data_pdf/cat/ly_ds_e_5_11_csm54.pdf?id=949 >. Viewed 1.4.2022.

76 Achat, S; Teisseyre, Y; Marode, E. 1992. The scaling of streamer-to-arc transition in a positive point-to-plane gap with pressure. Journal of Physics D: Applied Physics, 25(4). 661 – 668.

Appendix 1: Microscopic electrode surface analysis – plasma-type discharge with 2 mm electrode gap

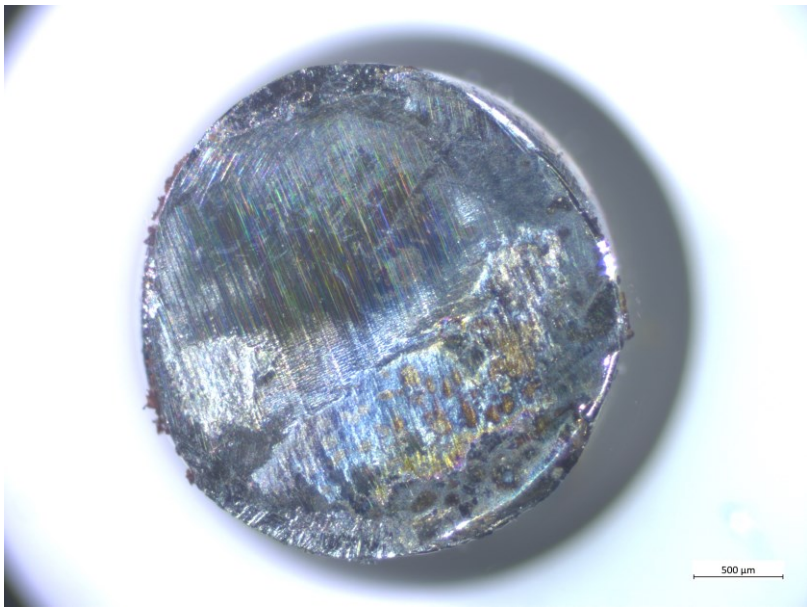

Figure 1. View of NGK BP5ES spark plug's anode after firing of three plasma-type discharges with the discharge capacitor charged to 200.0 VDC. Discharge energy before losses was 1.12 J. Gap between the electrodes was 2 mm.

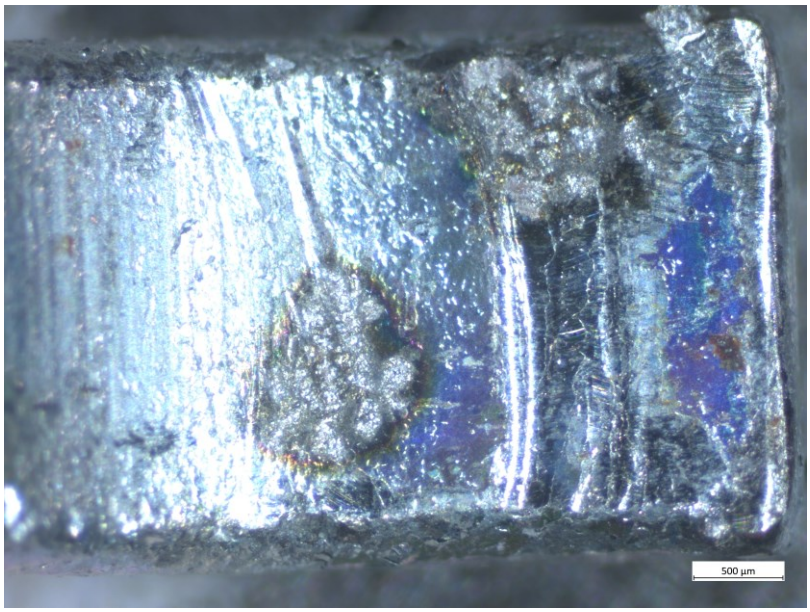

Figure 2. View of NGK BP5ES spark plug's cathode after firing of three plasma-type discharges with the discharge capacitor charged to 200.0 VDC. Discharge energy before losses was 1.12 J. Gap between the electrodes was 2 mm.